

Chiral bio-inspired plasmonics: a paradigm shift for optical activity and photochemistry

Oscar Ávalos-Ovando, Eva Yazmin Santiago, Artur Movsesyan, Peng Yu, Lucas Besteiro, Larousse Khosravi Khorashad, Hiromi Okamoto, Joseph M Slocik, Miguel A Correa-Duarte, Miguel Comesaña-Hermo, et al.

▶ **To cite this version:**

Oscar Ávalos-Ovando, Eva Yazmin Santiago, Artur Movsesyan, Peng Yu, Lucas Besteiro, et al.. Chiral bio-inspired plasmonics: a paradigm shift for optical activity and photochemistry. ACS photonics, 2022, 9 (7), pp.2219-2236. 10.1021/acsphotonics.2c00445 . hal-03795423

HAL Id: hal-03795423
https://hal.science/hal-03795423

Submitted on 4 Oct 2022

HAL is a multi-disciplinary open access archive for the deposit and dissemination of scientific research documents, whether they are published or not. The documents may come from teaching and research institutions in France or abroad, or from public or private research centers.

L'archive ouverte pluridisciplinaire **HAL**, est destinée au dépôt et à la diffusion de documents scientifiques de niveau recherche, publiés ou non, émanant des établissements d'enseignement et de recherche français ou étrangers, des laboratoires publics ou privés.

Chiral bio-inspired plasmonics: a paradigm shift for optical activity and photochemistry

Oscar Ávalos-Ovando[1,2], Eva Yazmin Santiago[2], Artur Movsesyan[1,2], Peng Yu[1], Lucas V. Besteiro[3], Larousse Khosravi Khorashad[4], Hiromi Okamoto[5], Joseph M. Slocik[6], Miguel A. Correa-Duarte[3], Miguel Comesaña-Hermo[7], Tim Liedl[8], Zhiming Wang*[1,9], Gil Markovich*[,10], Sven Burger*[,11,12], and Alexander O. Govorov*[,2]

[1] Institute of Fundamental and Frontier Sciences, University of Electronic Science and Technology of China, Chengdu 610054, China

[2] Department of Physics and Astronomy, Ohio University, Athens, Ohio 45701, United States

[3] CINBIO, Universidade de Vigo, 36310 Vigo, Spain

[4] Department of Electrical & Computer Engineering, University of Nebraska−Lincoln, Lincoln, Nebraska 68588, United States

[5] Institute for Molecular Science and the Graduate University for Advanced Studies (SOKENDAI), Okazaki, Aichi, Japan

[6] Soft Matter Materials Branch, Materials and Manufacturing Directorate, Air Force Research Lab, Wright Patterson Air Force Base, Ohio 45433-7750, United States

[7] CNRS, ITODYS, Université Paris Cité, F-75013 Paris, France

[8] Faculty of Physics and Center for NanoScience (CeNS), Ludwig-Maximilians-University, 80539 Munich, Germany

[9] Institute for Advanced Study, Chengdu University, Chengdu 610106, China

[10] School of Chemistry, Raymond and Beverly Sackler Faculty of Exact Sciences, Tel Aviv University, Tel Aviv, 6997801 Israel

[11] Zuse Institute Berlin, 14195 Berlin, Germany

[12] JCMwave GmbH, 14050 Berlin, Germany

* Corresponding authors: zhmwang@gmail.com, gilmar@tauex.tau.ac.il , sven.burger@jcmwave.com , govorov@ohio.edu

Keywords: Chiral plasmonics, chiral nanocrystals, bio-assembly, photochemistry, circular dichroism, DNA origami

Abstract:

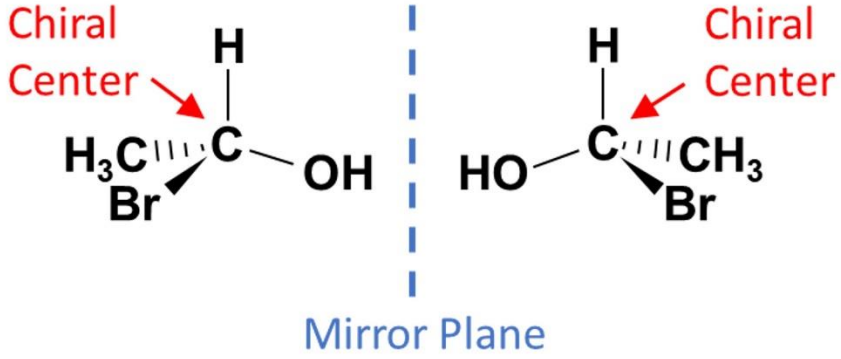
This Perspective concerns the latest developments in the field of chiral nanocrystals (NCs) and metastructures, focusing primarily on plasmonic nanostructures. Such nanomaterials exhibit unusually strong near-field and electromagnetic responses that enable efficient biosensing and light manipulation. Herein we share our thoughts on the latest trends that mark what we call a paradigm shift for the vast and dynamic field of chiroptical materials. The topics to be considered include polarizationsensitive photocatalysis with chiral plasmonic NCs, chiral bioconjugates, DNA-based assemblies, chiral growth, and we also describe the fundamental challenges for optical induction of chirality, transfer of chirality between different scales, and theoretical issues that nanoscience is facing.

Chirality is a purely geometric concept, but it is at the heart of modern chemistry.[1] Why so? Since our coordinate space at a given time instant includes only three dimensions, we can always create from an object with no mirror symmetry another state by the mirror-image operation. This mirror-imaged object is, in fact, a new one since it cannot be superposed with the initial shape by any rotations or translations. Such a pair of mirror-imaged objects is regarded by scientists as enantiomers or two chiral states of one molecule (Figure 1a). In this molecule (1-bromoethanol, C_2H_5BrO), the central atom is called a chiral center. In chemistry, any carbon atom - that has four different substituents forming a tetrahedral - is a chiral center. Naturally, since life is carbon-based, such chiral centers are found everywhere. Optical spectroscopy that senses the chiral states is called circular dichroism (CD). It employs chiral states of light, i.e., the right- and left-circularly polarized (RCP and LCP, respectively) photons (Figure 1b), and it is defined as

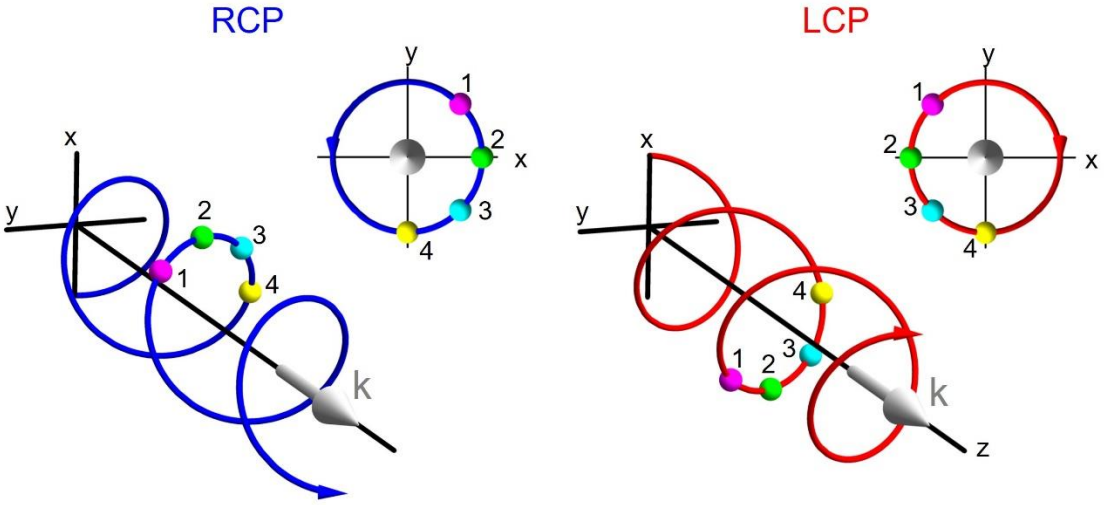
$$CD = A_{\mathrm{LCP}} - A_{\mathrm{RCP}}$$

where A_{LCP} and A_{RCP} are the absorbencies. Figure 1c shows a typical example of experimental data. The graph depicts the UV signal of unordered polypeptides, which nevertheless possess consistent and reproducible CD. It is important to note that the collection of chiral objects is in solution at random orientations (Figure 1c).

a Structural (static) chirality



b Electromagnetic chirality



c The CD spectroscopy approach: solution

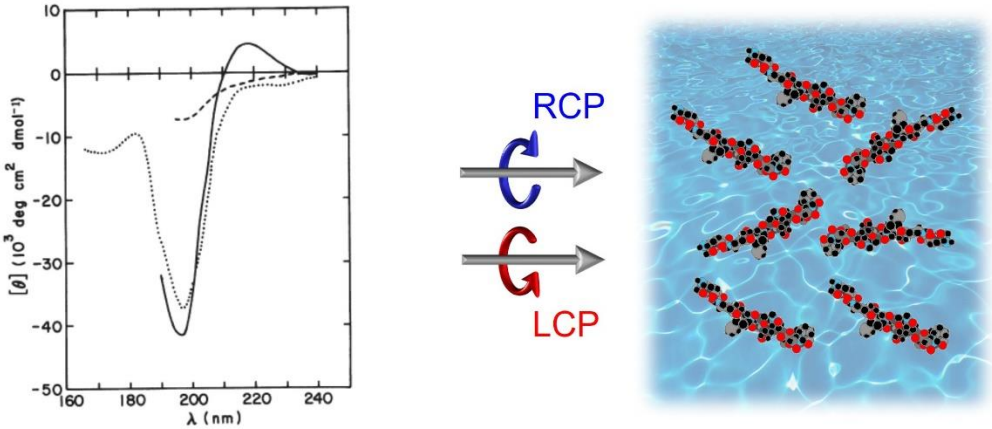


Figure 1: Chirality concepts. *(a) Example of structural chirality: two enantiomers of a molecule, i.e. two different molecules that are distinguishable from its mirror image. (b) Electromagnetic chirality: right-circularly polarized (RCP) and left-circularly polarized (LCP) light beams, shown in blue and red respectively, with a propagation direction (gray arrow) along the z-axis. Top views show xy-plane projections of electric vector sums along points of the beam, demonstrating that the tip of the vector follows a circular path, orthogonal to the direction of propagation. An observer set at the z-axis looking towards these views, will see a counterclockwise sense (RCP, blue) or a clockwise sense (LCP, red) of electric field rotation. Lower panels show panoramic views of the circularly polarized light (CPL) beams, which will look like a right-handed (RCP, blue) or a left-handed (LCP, red) helix. (c) Concept of a polypeptides solution's chirality being measured by LCP and RCP spectroscopy (right panel), which difference yields the circular dichroism (CD=LCP-RCP). If the solution components are chiral, CD≠0, as shown on the left panel for three different polypeptides solutions: Poly(Lys) (solid line), Poly(Ser) (dashed line), and Poly(Lys-Leu) (dotted line). Copyrights for panel b, modified from*[2]*. Copyrights for panel c*[2]*.*

This Perspective aims to discuss the latest developments in artificially designed chiral nanostructures, both biological and abiological, addressing their optical properties, photophysics, and photochemistry. Why are chiral nanomaterials so exciting, attracting so much interest? They can be made as the so-called bio-conjugates assemblies of inorganic nanocrystals (NCs) and biological elements with special geometries. The inorganic plasmonic elements of such bio-assemblies, i.e., NCs, are able to concentrate light inside small volumes and, in this way, greatly enhance the interaction between biomolecule and light. The optical CD lines in such plasmon-biomolecule complexes appear in the visible and can be used for sensing. In plasmonic NC

complexes with chiral geometries, the NCs interact with each other via ultra-strong plasmon-plasmon coupling, creating anomalously high CD signals. The nanomaterials of this kind involve both exciton-plasmon and plasmon-plasmon interactions. This mini-review covers a large set of selected topics, such as the plasmonic induction of chirality in bio-assembly, chiral NCs assemblies, polarization-sensitive plasmonic photochemistry and chemical applications of a reaction, and 2D/3D models of chirality, among others.

Plasmonic induction of bio-chirality.

We start with a single biomolecule. A quantum formula for CD of a chiral biomolecule reads[3]

$$CD_{\text{molecule}} \propto \text{Im}\left[\vec{\mu}_{12} \cdot \vec{m}_{21}\right] \qquad (1)$$

where $\vec{\mu}_{12}$ and $\vec{m}_{21}$ are the quantum matrix elements of the electric and magnetic dipole moment operators of a chiral biomolecule. As seen from eq 1, an optically active molecule should have the dipole moments in the configuration $\vec{\mu}_{12} \cdot \vec{m}_{21} \neq 0$, i.e., the dipoles should not be perpendicular to each other (Figure 2a). Furthermore, the formalism leading to eq 1 assumes the averaging over six directions of incidence, as illustrated in Figure 2a.

In the next step, we look at the response of a chiral molecule in the presence of a plasmonic NC. Figure 2b presents modeled theoretical data for this case from Ref. [4]. A chiral molecular dipole has a resonance in the UV at 200 nm, and its CD and ORD signals show the corresponding characteristic spectral lines (Figure 2b, upper graph). For a review on chiral molecular spectroscopy, we recommend the reader to see a classical text edited by Fasman.[2] In a molecule-NC complex, the electric dipole moment can be either normal or tangential to the surface, and this will influence the exciton-plasmon interaction. Figure 2b (lower panel) shows that the exciton-plasmon interaction is the strongest in the normal orientation. The theory for the chiral plasmon-

exciton interaction can be found in Refs.[5–7] Mathematically, the following equations describe the above effects for a single chiral dipole attached to a plasmonic sphere

$$CD_{\text{total}} = CD_{\text{molecule}} + CD_{\text{plasmon-induced}} \qquad (2)$$

where the second contribution comes from the exciton-plasmon interaction. We also note that the total CD is a simple sum of two terms since this signal originates from absorption inside the components. The first term, CD_{molecule}, is given by Eq. (3)

$$CD_{\text{molecule}} \propto \text{Im}\left[\left(\hat{P}_{\text{plasmon}} \cdot \vec{\mu}_{12}\right) \cdot \vec{m}_{21}\right] \cdot \frac{\Gamma}{\left(\text{h}\omega - \text{h}\omega_0\right)^2 + \Gamma^2} \qquad (3)$$

where the second factor in eq 2 is in fact the absorption line-shape of the molecule, in which $\text{h}\omega_0$ and Γ are the energy and the broadening of the molecular transition; $\hat{P}_{\text{plasmon}}(\omega)$ is the plasmonic enhancement matrix of the chiral molecule in the hybrid. The plasmonic enhancement matrix is strongly distance-dependent, and, for the dipolar limit of the molecule-plasmon interaction, $\hat{P}_{\text{plasmon}} \propto 1/d^3$, where d is the molecule-NC center-to-center separation. Thus, as the molecule-NC distance increases, the plasmon enhancement gradually decreases. The second term in eq 2 is of a different origin: this plasmon-induced CD comes from the light dissipation inside the plasmonic NC and, in general, it has a complex mathematical structure. Rationalizing both analytical and numerical results,[4–7] the plasmon-induced can be written as eq 4

$$CD_{\text{plasmon-induced}} \propto \text{Im}\left[\varepsilon_{\text{NP}}(\omega)\right] \cdot f_{\text{mol-res}}(\omega) \cdot \text{Im}\left[\left(\hat{K}_{\text{plasmon}} \cdot \vec{\mu}_{12}\right) \cdot \vec{m}_{21}\right] \qquad (4)$$

and

$$f_{\text{mol-res}}(\omega) = \frac{\left(\text{h}\omega - \text{h}\omega_0\right)}{\left(\text{h}\omega - \text{h}\omega_0\right)^2 + \Gamma^2}$$

where $\varepsilon_{NC}(\omega)$ is the dielectric function of the metal. Then, $\hat{K}_{plasmon}$ is a near-field matrix with a complex structure describing the interaction between the molecular dipole and the local plasmonic fields inside the hybrid; this matrix includes a strong plasmon enhancement effect and also the effects of hot spots.[8] A function $f_{mol\text{-}res}$ incorporates the resonant effects of the molecule. All factors in eq 4 are strongly size-, distance-, frequency-, and geometry-dependent. For example, the plasmonic matrix contains a resonant factor that can lead to giant intensities of CD signals when a chiral molecule is placed in a plasmonic hot spot.[6,8–10] Regarding the distance dependence, $\hat{K} \propto a^3 / d^3$ for the simplest model (a single spherical NC); here *a* is the NC size.

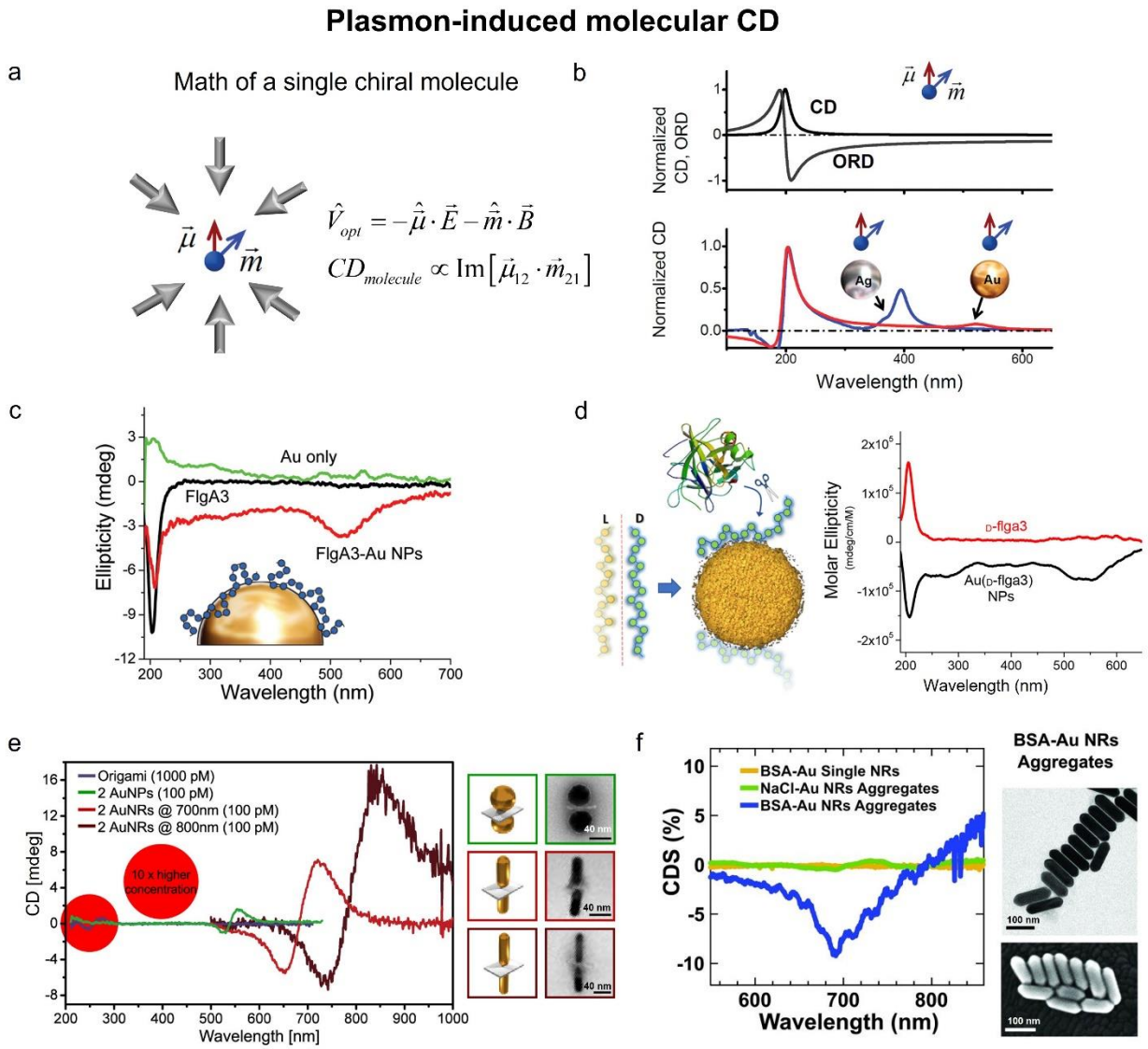


Figure 2: Plasmon-induced molecular circular dichroism. *(a) Chiral biomolecule with its quantum matrix elements of the electric ($\hat{\vec{\mu}}_{12}$) and magnetic ($\hat{\vec{m}}_{21}$) dipole moment operators, being tested with light over six directions of incidence. (b) Circular dichroism (CD) and optical rotatory dispersion (ORD) responses of a chiral molecule (upper panel) and calculated CD responses of two molecular-plasmonic assemblies (lower panel). (c) CD spectra of gold nanoparticles functionalized with the FlgA3 peptide, inducing a pronounced response at ~520nm in the UV region. (d) Concept of L- or D-peptides functionalizing a gold NC and of proteolytic cleavage of*

D-peptides via gold-mediated inversion of peptide chirality (left panel), and CD spectra of free D-flga3 peptide and after synthesis of gold NCs (right panel), showing the chiral restructuring of the functionalized D-flga3 peptide. (e) Three nanoantennas in a solution composed by different size/shape metallics NP dimers connected by a DNA-origami template (right panels), and CD measurements (left panel) of a typical two-layered DNA origami sheet at the UV region (black line), signal which is shifted to the red and enhanced by the metallic antennas 30-fold (green line) and 300-fold (red curves). (f) Circular differential scattering (CDS) spectroscopy of gold nanorod (Au NR) with NaCl-induced and bovine serum albumin (BSA)-induced aggregates (left panel); and on the right panel, TEM (top) and SEM (bottom) images of the BSA mediating predominant side-by-side assembly of Au NRs. Copyrights for panel b[4]*. Copyrights for panel c*[11]*. Copyrights for panel d*[12]*. Copyrights for panel e*[8]*. Copyrights for panel f*[13]*.*

Figure 2b-d shows a few prominent experimental examples of the plasmonic induction effect. Figure 2c and 2d present classical results on the peptide-conjugated spherical NCs from Refs.[11,12] One can see the appearance of the plasmon-induced CD signals at the plasmonic peak wavelength. The sign of the plasmonic CD corresponds to the biomolecular dipoles in the normal configuration. The chemical and photophysical mechanisms of interaction in a bio-conjugate are rather complex and may involve conformations as one can see from panel d; the use of synthetic peptide with the opposite chirality gives a surprising result: its optical chirality is inverted upon the conjugation with an Au NC. Probably, the most controlled and complex assemblies can be made using the DNA origami approach (Figure 2e). One can see how the assembly of two nanorods (NRs) creates giant CD signals coming from the chiral DNA molecules located in such a hot spot. Figure 2f presents a unique experiment on single-particle spectroscopy measuring the

so-called far-field CD scattering (CDS). One can see that an assembly with chiral bio-linkers shows prominent CDS, which can be interpreted as a plasmonic induction of chirality in the NRs due to the exciton-plasmon interaction and hot spots. Current literature has now a large number of observations of plasmon-induced CD, and we can refer the reader to several reviews devoted to this topic.[10,14–17]

Plasmonic NC assemblies and the origin of chirality.

The second major mechanism of plasmonic CD is the plasmon-plasmon interaction.[18] An inspiration for this mechanism came to us from the helical molecular structure of some biomolecules. One famous example is a DNA molecule with its chiral helical geometry (Figure 3a). Another prominent case an α-helix protein (Figure 3b,c). In the latter example, the chiral UV response comes from the excitonic transitions localized on the so-called peptide bonds, i.e., junctions between the individual amino acids (Figure 3b).[2] The theory of the helical CD mechanism of molecular helices[2] was developed by Moffitt in his seminal work, Ref. [19]. In NC assemblies, one can achieve an analogous effect when the spherical NCs are placed on a helical line, Figure 3d,f,g. Chiral NC assemblies can be with various chiral geometries including tetrahedral (Figure 3e)[20,21] and pyramidal organizations.[18,22] The resulting objects with chiral organizations exhibit very characteristic and strong plasmonic CD. Optical chirality and strong CD originate from the chiral organization and the plasmon-plasmon interactions in a complex comprised of nonchiral NCs. In the dipole limit of the NC-NC interaction, the plasmonic CD behaves in the following way

$$CD_{\text{plasmon-plasmon, nanocrystal}}(\omega) \sim \frac{a^{12}}{R^{8}} \qquad (5)$$

where a and R are the NC diameter and the inter-nanoparticle distance, respectively. We observe from eq 5 that the plasmonic CD strength critically depends on both the NC-NC distance in a complex and on the size of the NCs. The plasmonic CD signal, if expressed in the standard units of $M^{-1}cm^{-1}$, is much greater (many orders of magnitude) than any molecular signal.[23] The physical reasons for so extraordinary strong plasmonic signals come from the fundamental properties of metal NCs. First, plasmonic NCs have large numbers of free electrons and, second, those NCs strongly interact. Overall, the CD strength of plasmonic assemblies strongly depends on the scaffold geometry.[18]

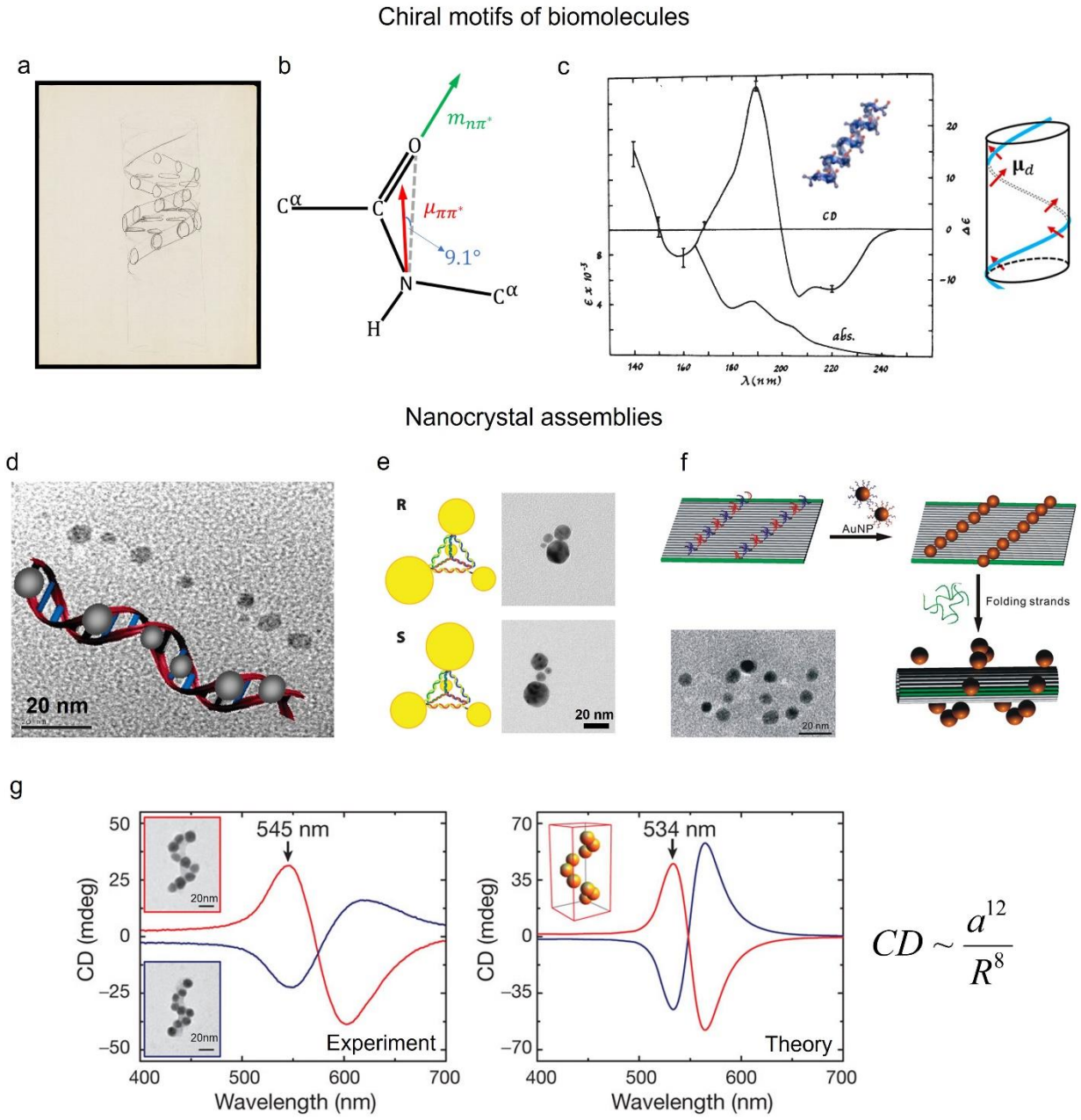


Figure 3: Chiral assemblies of biomolecules and metallic nanocrystals. *(a) Original pencil sketch of the DNA double helix by Francis Crick. (b) The electric dipole transition moment of the amide* $\pi\pi^*$ *transition (*$\mu_{\pi\pi^*}$*) and the magnetic dipole transition moment of the amide* $n\pi^*$ *transition (*$m_{n\pi^*}$*). (c) Absorption and CD spectra of poly-*γ*-methyl glutamate in hexafluoro-2-propanol (left panel); inset shows the molecular structure of an* α *-helix protein. The right panel*

shows a model of the α-helix with optical dipoles. (d) TEM image and model of silver NCs grown on poly(dG)-poly(dC) double stranded DNA scaffold show sizable CD, whereas in the absence of the scaffold CD is not seen. (e) Models and TEM images of pyramidical DNA-gold systems, in their R- (top panels) and S- (lower panels) configurations. (f) Schematics of the construction of 3D plasmonic DNA origami dressed in chiral gold NCs in a helical arrangement, and the resulting TEM image (lower left panel). (g) CD measurements (left) and simulations (right) of self-assembled gold nanohelices with left-handed (red curves) and right-handed (black curves) chirality, as shown in the TEM images/models insets. Dipole theory predicts strong CD signals when the NCs are either large or arranged in a tighter helix $CD: a^{12}/R^8$, with a the NP radii and R the helix radii. Copyrights for panel a. Copyrights for panel b, modified from[2]*. Copyrights for panel c, modified from*[24] *and* [25]*. Copyrights for panel d*[26]*. Copyrights for panel e*[20]*. Copyrights for panel f*[27]*. Copyrights for panel g*[23]*.*

Although, the most exciting system with a helix motif to look at is a plasmonic helix with a variable number of spherical NCs, namely N_{NC} (Figure 4). First, such structures were described by us theoretically in Refs. [18,28]. The physics of chiral responses of a NC helix is rather interesting. Since our coordinate space is 3D, nonzero CD signals should appear starting from $N_{\mathrm{NC}} = 4$ (Figure 4a). For small numbers of N_{NC}, the regime is near-field and the dipolar plasmon-plasmon interaction dominates. For large N_{NC}, we enter, of course, the electrodynamic regime of interaction,[28] like in the Moffitt's model of the α-helix protein.[2] From the very beginning,[18,28] it was very tempting to check out the plasmonic helix theory. Figure 4 shows such experiment. As usual, an experiment should bring something surprising, and it did! We indeed observe a prominent

CD threshold for $N_{NP} \geq 3$ (Figure 4b). The experiments were done with two kinds of helices. For the "fat" helix with a small vertical pitch (SPH), the CD amplitude should strongly oscillate as a function of N_{NC} with the period of 4. For the "normal" helix with a long vertical pitch (LPH), we should observe a clear threshold at $N_{NC} = 4$ and then a monotonic rise till the helix lengths $L_{helix} : \lambda_{plasmon}$. Indeed, we see such trends impressively for the interval $N_{NC} = 1-7$. Moreover, it is exciting to observe that the CD threshold is never abrupt! Both kind of helices in Figure 4b demonstrate it. Two reasons for this interesting effect can be the following. The 1st mechanism, which was actually computed in that study,[29] is the dielectric-plasmon interactions in an assembly made of a dielectric DNA cylinder and Au nanospheres. Geometrical chirality in this case is present also for the cases $N_{NP} = 2$ and 3. Indeed, the theory review such signals. Simultaneously, the case $N_{NC} = 1$ stays no-chiral (Figure 4c, right). In Figure 4d, we show the electromagnetic fields in such systems. The mechanism #2, which may exist in this state and was already discussed on Figure 2, is the exciton-plasmon interaction, i.e., the interaction between plasmonic NCs and chiral DNA molecules. Ref. [29] did not compute this contribution to the CD signals, which needs a different approach based on the local bio-chiral parameter.[30]

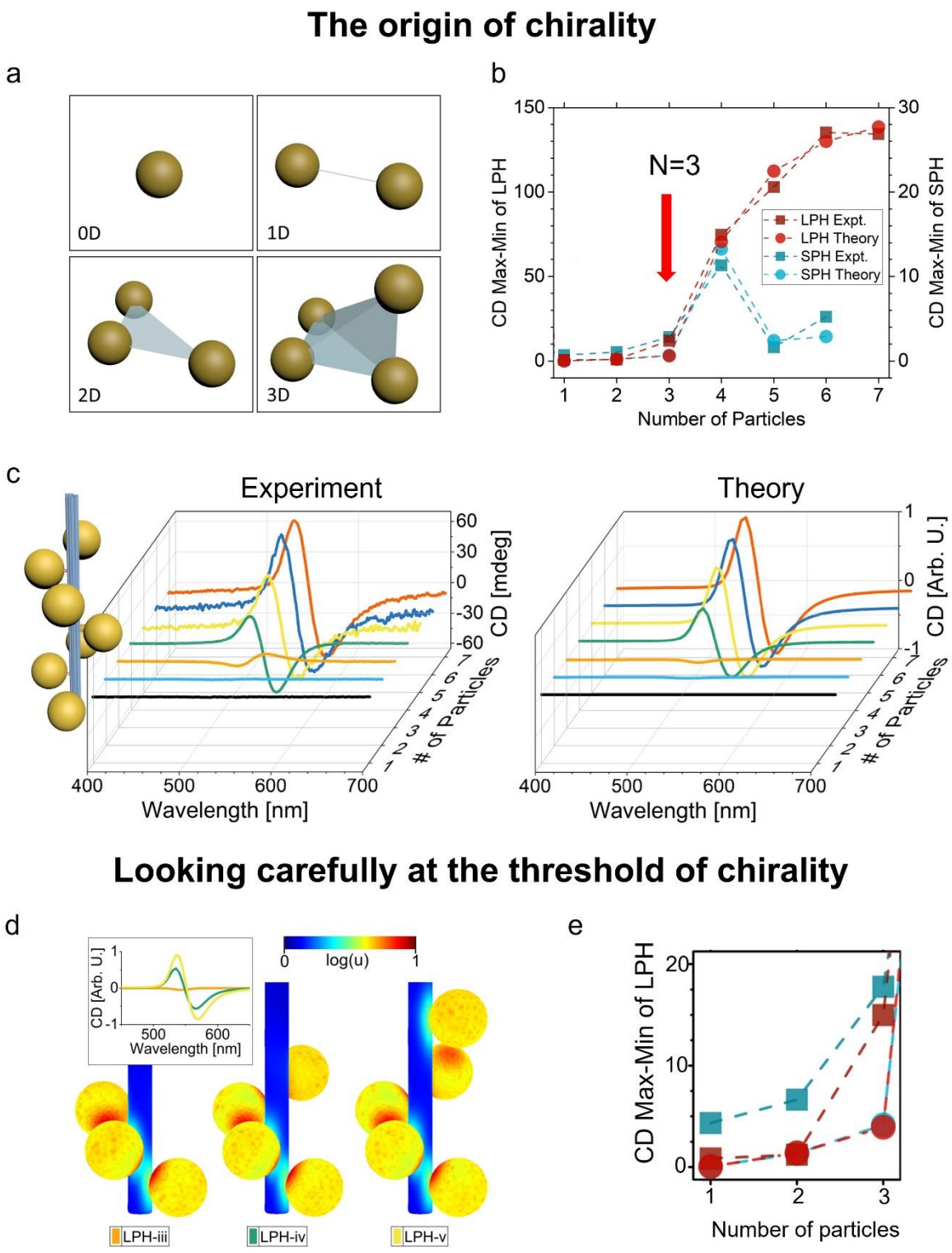


Figure 4: Origin of chirality in plasmonic meta-molecules*. (a) Different arrangements of spherical NCs: 0D, 1D and 2D arrangements do not induce chirality, whereas 3D arrangement does. (b) and (c) Emergence of chirality for N=3: (b) Differences between the maximum and*

minimum of the CD at two kinds of structural-different helixes, a small pitch helix (SPH) and a large pitch helix (LPH); (c) CD spectra of different LHPs, each with increasing number of spherical NCs. (d) Simulated optical field energy density u *of three different samples of LPHs, shown as pseudo-colors on the surfaces of Au NCs (yellow spheres) and on the dielectric DNA rods (blue cilinders), and corresponding CD spectra (inset). (e) Same as panel (b) but zoomed, showing the jump in maximum CD when one arranges 3 NCs in a helical configuration, as shown in the leftmost case of panel (d). Copyright for all these panels*[31].

3. Chiral monolithic nanocrystals, chirality transfer between the scales, and related historic remarks.

The concept of enantiomers observed and formulated by Louis Pasteur in his genius reports from 1848 and 1849[32,33] is a simple reflection of the fact that our world is 3D. Interestingly that the word "chiral" itself was coined later, by Lord Kelvin in 1894.[1] It was indeed a revolutionary observation for chemistry and especially for biochemistry. Tartaric acid studied by Louis Pasteur (Figure 5a,b) is a chiral molecule, forming two kinds of macrocrystals (i.e., a pair of enantiomers) with chiral and well-defined shapes (Figure 5b). In other words, the chiral structure at the molecular level becomes reflected on the microscopic structure visible by the naked eye. By the way, this molecule is largely involved in the chemistry and technology of wine. The geometry of a chiral molecule is often nontrivial, but still can be described as two enantiomers. For a screw, the description is more formalized in terms of mathematical definitions – here we just talk about right- and left-handed (RH and LH) helices (Figure 5c).[34]

Now returning to NCs, colloidal NCs made of the most popular noble materials (Au and Ag) are typically achiral since the bulk lattices of these metals are not chiral. Although, such NCs

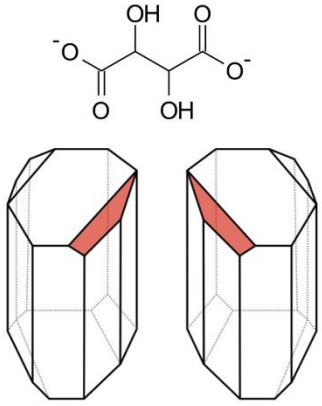
can be strongly anisotropic and often possess very interesting shapes (Figure 5d-f). However, the field of colloidal NCs is so active and includes thousands of enthusiastic chemistry groups, and it was clear that chiral colloidal NCs should appear sooner or later (Figure 5g-j). Figure 5g shows one of the early examples, with chiral Ag nanorods forming a racemic ensemble.[35] It could be that those shapes were found in Ref. [35] non-intentionally. Later, the search for chiral shapes was motivated by the following ideas. (1) There was the understanding that a chiral seed should be able to direct chiral growth under certain conditions.[36,37] (2) Our early calculations[38] have shown strong and characteristic optical CD from plasmonic NCs with chiral surface patterns, like shown on Figure 5k. Indeed, in the set of impressive experiments at Tel Aviv University,[36,37] chiral growth was directed by small chiral amino acids, resulting in enantiomerically pure solutions of NCs with chiral crystal lattices, or chiral shapes, or both. (Figure 5h,i). Lately, amazing chiral cuboids with ultra-strong CD were fabricated using the peptide-based colloidal chemistry (Figure 5j).[39] As one concluding remark for this section, we note that while Pasteur's famous experiment was done by sorting RH and LH macrocrystals by a tweezer, the fabrication of chiral NCs involves initially chiral seeds and, in this way, results in colloidal solutions with large enantiomeric excesses and strong CD signals. Chirality, in this case, originates from a bio-molecular seed and, in fact, gets borrowed from nature again.

The idea of enantiomers

a



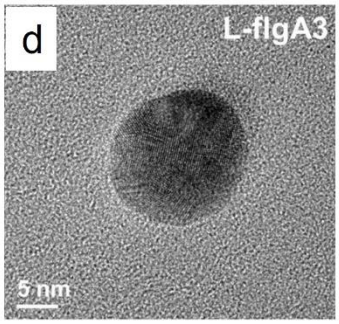
b

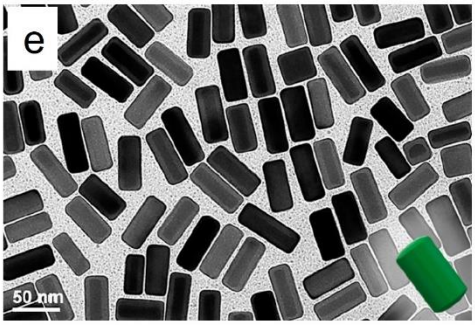


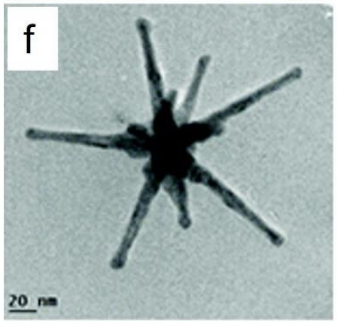
c

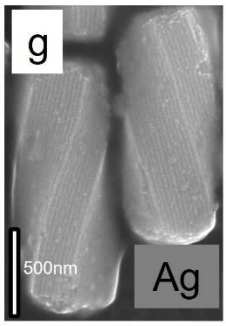


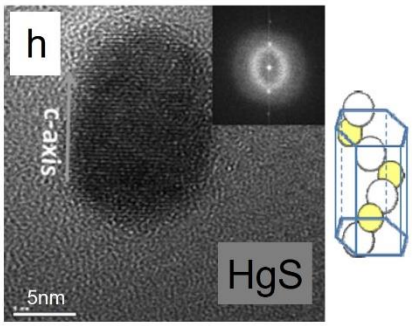
Colloids

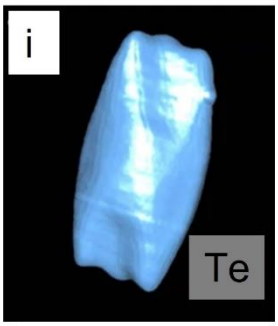


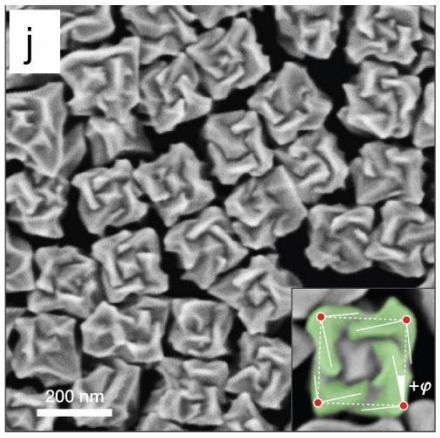












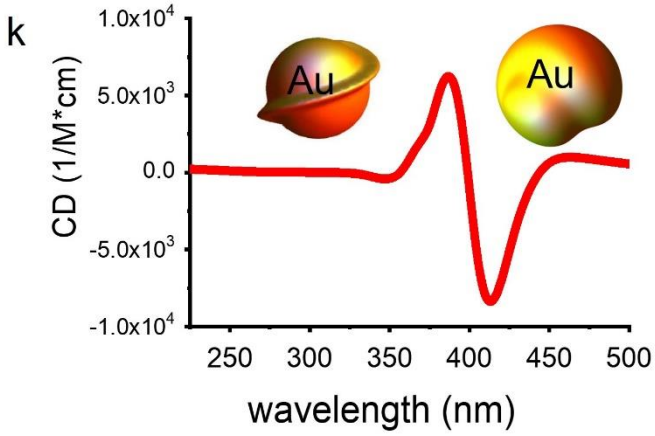


Figure 5: Enantiomers and colloidal assemblies. *(a) Louis Pasteur in 1857. In 1848, he solved the tartrares problem of panel (b), the first demonstration of molecular chirality: the optical activity related to the shape and composition of crystals was responsible for twisting the light. (b) Top: Chemical enantiomer: a chiral molecule. Bottom: Crystallographic enantiomer: the dextrorotatory (left) and levorotatory (right) sodium ammonium tartrate crystal. (c) A geometric enantiomer: two corkscrews, one left-handed and one right-handed. (d) HR-TEM images of Au NCs synthesized with the peptide L-FlgA3. (e) TEM image of Au-core/Ag-shell nanorods. (f) Gold six-spikes nanostars with 100 nm spike lengths. (g) SEM image of Ag nanoprisms displaying helical assemblies upon slow evaporation of its dispersion. (h) TEM image of individual a mercury sulfide nanocrystal (left), and schematic illustration of the nanocrystal's unit cell consisting on single helices with opposite chirality (right). (i) Tomographic reconstruction from a dark-field STEM image of a Tellurium NC, showing structural chirality in the twisted ridges crossing diagonally between vertices at the two ends. (j) SEM image of 3D plasmonic helicoids synthesized using D-cysteine, where the inset highlights the tilted edges (solid white lines), the cubic outline (dashed white lines) and the tilt angle (+ φ). (k) Models of gold twister and anti-twister (size ≈14 nm) and their CD spectra with maximum structural perturbation of 1.5 (left) and 0.8 nm (right). Copyright for panel a. Copyright for panel b. Copyright for panel c. Copyright for panel d*[12]*. Copyright for panel e*[40]*. Copyright for panel f*[41]*. Copyright for panel g*[35]*. Copyright for panel h*[36]*. Copyright for panel i*[37]*. Copyright for panel j*[39]*. Copyright for panel k*[38]*.

4. Local chirality, functional Chiral nanostructures and plasmonic nanotechnology.

Measuring local chirality is an interesting task and represents a novel type of spectroscopy (Figure 6a).[42,43] Even a nonchiral nanostructure (like a plasmonic slab in Figure 6a) will demonstrate a

local chiral response since the incident beam is CP (LH or RH), and chirality comes from the electromagnetic wave itself (see Figure 1b). In such situations, the interplay of a nonuniform nanostructure geometry and the tip's geometry plays a major role in creating far-field chiral responses (Figure 6a, right). A review on several CD techniques of this kind can be found in Ref. [42]. Later, the idea of creating local chiral field patterns has been very productive in several other ways as outlined here below. Figures 6b and 6c show two cases of induction of chirality by circularly polarized light (CPL) in a nanostructure. The first case utilizes surface photochemistry inside a solution (Figure 6b), and the second example is based on plasmon-induced polymerization (Figure 6c). Interestingly, both nanostructures used in (b) and (c) are achiral, and the resulting chiral patterns occur due to the CPL. Next, Figures 6d-f shows the principles and related examples of local photothermal chirality and its imaging. Local CD and its g-factor for the chiral phototemperature induction was introduced by us in Ref. [44] as

$$CD_T(\vec{r}) = \delta T(\vec{r}) = \Delta T_{\mathrm{LCP}}(\vec{r}) - \Delta T_{\mathrm{RCP}}(\vec{r})$$

$$g_T = \frac{\Delta T_{\mathrm{LCP}}(\vec{r}) - \Delta T_{\mathrm{RCP}}(\vec{r})}{\left[\Delta T_{\mathrm{LCP}}(\vec{r}) + \Delta T_{\mathrm{RCP}}(\vec{r})\right]/2}$$

A few impressive demonstrations lately (Figure 6e,f) revealed the possibility to observe local plasmonic photothermal patterns with the aid of careful confocal optical imaging.[45,46]

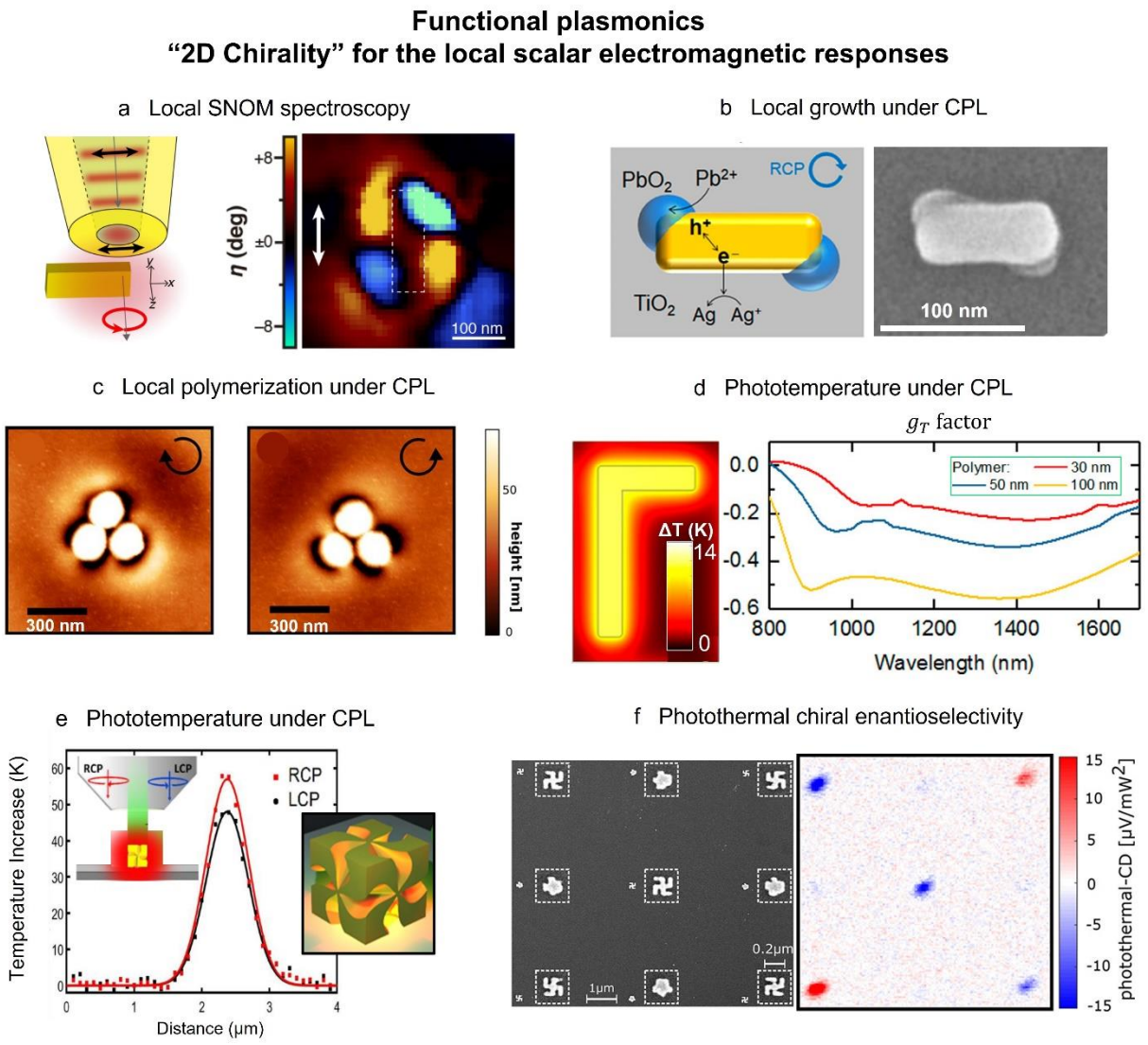


Figure 6: Local functional plasmonics. *(a) An achiral gold rectangular prism illuminated with linearly polarized light, will generate local circularly polarized field (left panel), which can be visualized via scanning near-field optical microscopy (SNOM) imaging (right panel). (b) Another achiral gold rectangular prism illuminated with CPL, will generate a chiral local hot-electrons response which leads to local growth at those regions, as schematically shown (left panel) and its correspondent SEM image (right panel). (c) AFM images of gold metamolecules composed by a 2D triangular arrangement of three gold nanodisks embedded in a photosensitive azobenzene-containing polymer (PAP), after RCP (left panel) and LCP (right panel). The maps show mirrored*

differences in the PAP, probing its sensitivity to the handedness of the light via the achiral metamolecule, hence converting this achiral structure into a geometrically chiral structure due to matter displacement. (d) Photoinduced temperature of a chiral gold metastructure on top of a polymer upon LCP illumination (left panel), and g-factor spectra for different polymer thicknesses (right panel), showing a significant chiral response of the system for generating photoinduced temperature. (e) Experimental observation of photothermal chirality in gold nanoparticle helicoids (right model), for the setup shown in the inset: CPL illumination creates different thermal profiles when scanning the distance through the helicoid. (f) High-resolution SEM images of a gammadion gold array (left panel), and corresponding photothermal CD images of the same SEM area (right panel), showing a clear sign change in the signal when recognizing the nanostructures chirality. Note achiral structures show a nearly zero CD signal. Copyright for panel a[47]*. Copyright for panel b*[48]*. Copyright for panel c*[49]*. Copyright for panel d*[44]*. Copyright for panel e*[46]*. Copyright for panel f*[45]*.*

5. Creating chiral objects with chiral light and the challenge of colloidal growth.

Plasmonic effects provide us with unique tools to realize anisotropic photo-growth of colloidal NCs.[50,51] The mechanisms of plasmonic growths involve enhanced electric fields, hot electrons (HEs), and phototemperature. This stream of research is very active nowadays in colloidal photochemistry. A recent review of the related mechanisms can be found in our forthcoming paper in *Advanced Optical Materials*.[31] Like optical experiments, photo-growth settings can be either planar or colloidal (Figure 7a,b). The planar model utilized directional illumination (Figure 7a), whereas the colloidal setting assumes NCs in liquid and at random orientations (Figure 7b). In the latter model, we need to illuminate our NC from all directions (Figure 7b). Of course, due to the

symmetry of the CPL, only anisotropic NCs can experience chiral distortion and growth under steady-state illumination. The idea of directional plasmonic photo-growth was impressively realized in Ref. [48] as illustrated above in Fig. 6b. The anisotropy of a NR in Ref. [48] in combination with the electromagnetic field of CPL creates a chiral pattern of surface plasmonic field leading to the local HEs generation near the surface. The latter triggers a surface reaction and growth. Figure 7 provides a dynamic theory for the topological properties of chiral photo-grown NCs.[52] Directional CPL illumination of a nanocube in panel (a) creates a 2D chiral distortion just as in the case of a NR in Ref. [48], with LCP and RCP light creating the formation of a 2D enantiomer pair (Figure 7a); note that we are talking here about 2D chirality and 2D enantiomers, since we deal with the directional light illumination and observe the x-y cross sections of the objects; in other words, we do not need to look at the z-dimension yet. The CPL illumination induces prominent 2D chiral shapes within our dynamic computational model, and the calculated directional CD profiles are also prominent and can be strong under certain conditions.[52] At this point, we need to note also that the overgrown nanocubes on Figure 7a exhibit strong and prominent 2D chirality, whereas 3D ("colloidal" or true) chirality remains very weak during the growth. This is the fundamental consequence of the interaction of a fast-moving and oscillating circular polarized wave with any nearly-static condensed-matter or molecular matter.

Now is the time to look at the colloidal case (Figure 7b). When illuminating from all directions, we no longer observe a chiral shape in the computation, nor 2D chirality nor 3D chirality. Although, some tiny chiral distortion must exist (from the symmetry arguments), but the computation did not catch it (this happens). We note that, in these computations, we can observe and quantify chirality by calculating directional (planar) and colloidal CD signals. The

vanishing CD signals in the colloidal setting are a fundamental property of the light-matter interaction. More discussion on this intriguing topic is in our recent papers.[52,53]

It is also instructional to investigate a different chiral growth regime when we start our computational photo-growth from a strongly chiral state (Figure 7c).[53] Computationally, it is less challenging, yet very interesting to look at. The initial plasmonic chiral property is so strong, and CPL will certainly be able to create two pairs of new enantiomers. However, in such a setting, we do not create chiral shapes from achiral matter, but we rather use NCs, which are chiral from the very beginning.

Chiral plasmonic photochemistry and growth: Challenges and opportunities

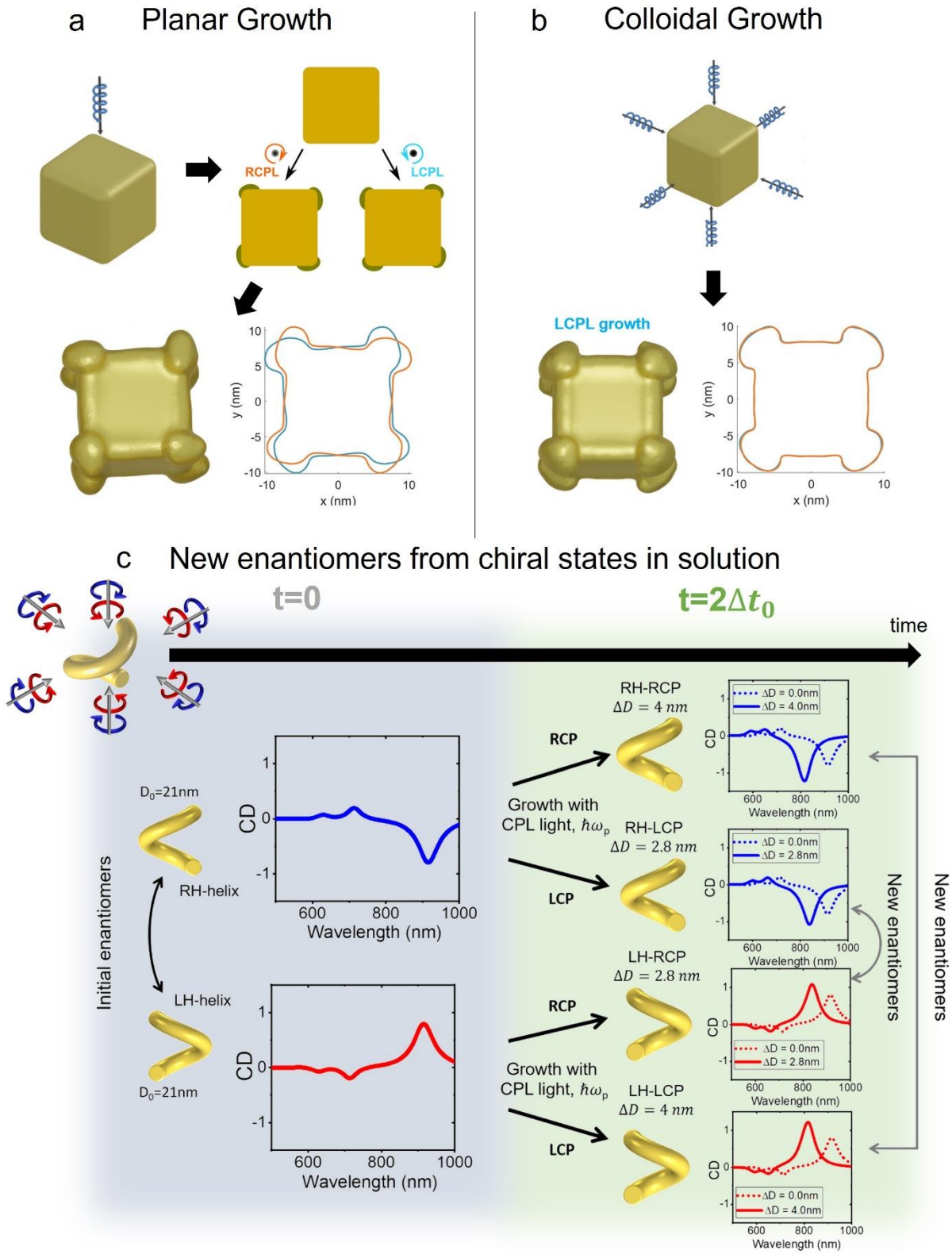


Figure 7: Chiral plasmonic photochemistry and photogrowth via local hot-electron induction. *(a) and (b) Illumination with CPL of a non-chiral gold cubical nanocrystal, either with (a) planar illumination, or (b) colloidal illumination in a solution. Top panels show schematic diagrams of CPL illumination, whereas lower panels show 3D and 2D views of calculations for the growth under LCP light, showing that planar illumination induces a truly chiral growth. (c) Schematic representation of a chiral gold helix being illuminated with CPL in a solution containing both enantiomers randomly oriented, and their evolution over time. Since in a solution, the components will be randomly oriented, an average over at least the six main orthogonal directions of incidence needs to be performed. At t=0 (gray region), both enantiomer within the solution can be characterized by their CD spectra. At* $t=2\,\Delta t_0$ *(green region), four final shapes could be growth depending on the initial enantiomer and the pumped CPL light at the plasmon resonance* ω_p*, shapes which can be characterized by their CD spectra. Copyrights for panels a and b*[52]*. Copyrights for panel c*[53]*.*

Chiral photochemistry at the molecular level has a long history.[54] Already the giants of molecular spectroscopy noticed and then coined the possibility to perform chiral (asymmetric) reactions with CPL. The pioneers of optical chirality, Le Bel and van't Hoff, described the chiral photochemical effect in their papers of ref [55] (1874) and ref [56] (1894), teaching us that CPL should be able to induce chiral chemical reactions. Then, the first successful asymmetric photoreactions were recorded by another forerunner in the field, W. Kuhn - his first studies on this topic appear in the late 1920s and early 1930s.[57,58] Here we take the liberty to recommend for the reader the text of Ref. [54] as an excellent review on the historical developments and concepts of chiral photochemistry. One crucial component in modern chiral photochemistry is the involvement of

the chiral chemical amplification effect,[54] which is to be addressed right in the next section. Finally, we should mention that, for colloidal NCs, the idea of CPL-driven photochemistry was employed recently in Ref. [59].

6. Polarization-sensitive hot-electron generation and plasmonic photochemistry with chiral nanostructures.

We already mentioned the challenge of the transfer of chirality between different scales. In chemistry, it happens in millions of instances starting from the most famous of observation by Louis Pasteur. In our field of research, plasmonic nanostructures create chiral fields so efficiently at the nanometer scale. However, at the molecular scale of a few Angstroms, the plasmonic electric fields are weakly chiral. One example is strong plasmonic hot spots in the NR-NR assembly in Ref. [8], shown in Figure 2e. Simultaneously, chiral plasmonic NCs should be able to create another kind of chiral photochemical phenomena – polarization-sensitive photochemistry in solution. The HE mechanism for this kind of chiral photochemistry is illustrated in Figure 8 and was recently realized in a challenging experiment by a joint Spanish-French team[60] (Figures 8c thru 8k). As described in the text of Ref. [54], the central problem for efficient chiral photochemistry is the small g-factors of chiral molecules that is, in fact, a fundamental property of the light-matter interaction in general. However, nature is going to favor us here - photochemical enantiomerization under CPL can be greatly enhanced due to the so-called chemical auto-amplification effect commonly observed in chiral catalysis[54] and catalysis in general. Indeed, the central observation in Ref. [60] is based on this effect. Whereas the g-factors of plasmonic ribbons in Ref. [60] are : 10^{-3} (Figure 8j), the photochemical g-factors for the polarization-sensitive reaction rates is ~1 (Figure8k).

Therefore, the observed chemical amplification factor is : 10^3 ! This chiral plasmonic photochemical effect certainly deserves further investigations and work towards applications.

Polarization-dependent photochemistry

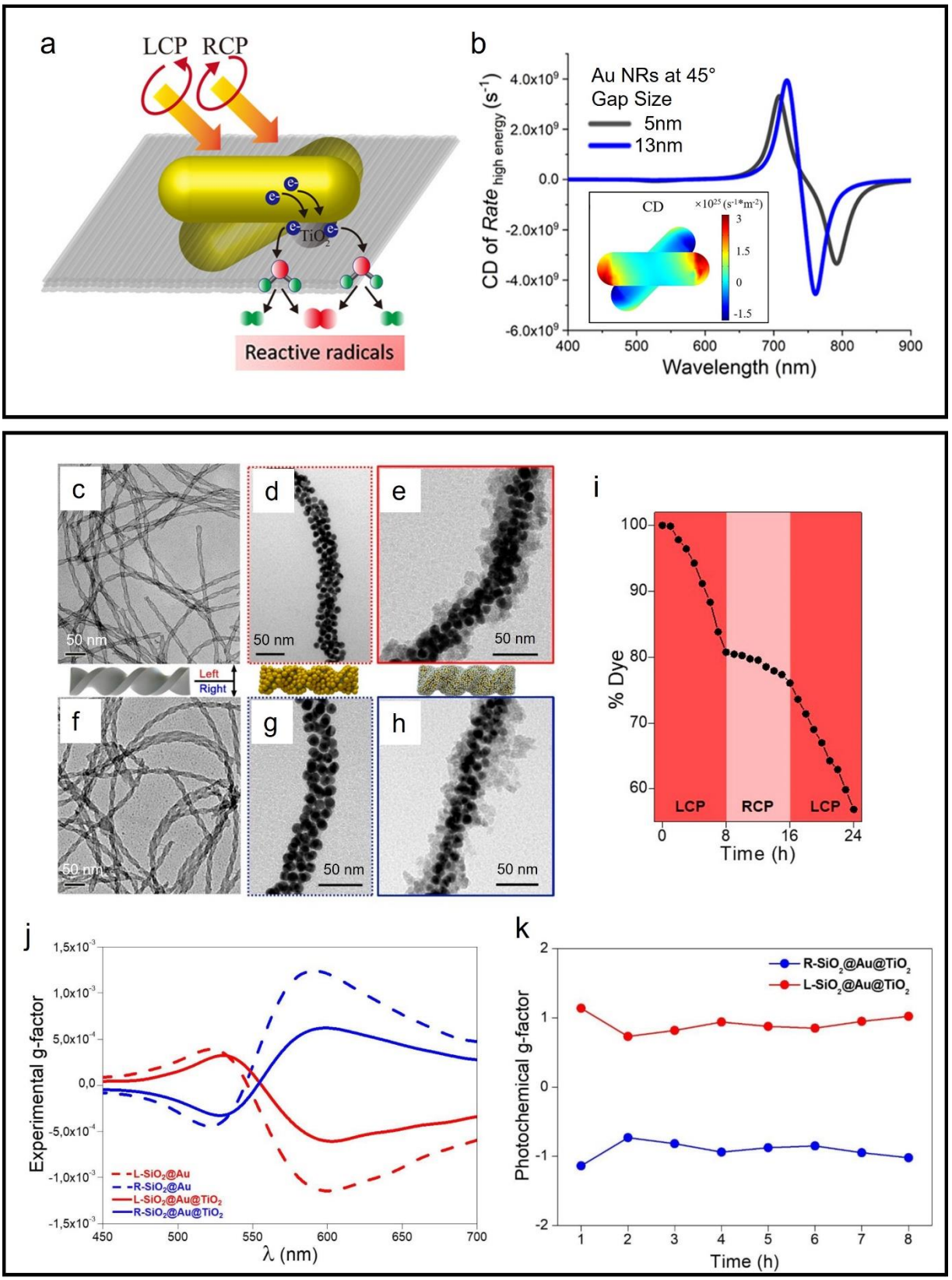


***Figure 8*: *Polarization-dependent photochemistry*.** *(a) Model of chiral plasmonic NRs dimers connected via a DNA origami template (gray) suspended in a water solution, under either LCP or RCP illumination. Hot electrons (HEs) are first injected into small TiO_2 nanocrystals on the gold surface, and later transferred to the solution, triggering the creation of reactive species able to catalyze some other reaction. (b) CD simulation of the averaged HE-generation for the system of panel (a), for NRs separated by 5nm and 13 nm gaps. The inset shows a map of the HEs generation for the 5nm gap system and an incident light propagating in the z direction with wavelengths of 710nm (Maximum CD). (c-h) TEM images of L-handed (c-e) and R-handed (f-h) nanoribbons composed of a twisted core of SiO_2 (c,f), an added first cover of Au NCs (d,g), and an added second cover of TiO_2 NPs (e,h), as indicated by the schemes in the middle panels. (i) Photodegradation of the organic dye rhodamine B (RhB) in the presence of left-handed hybrid nanoribbon of panel (e), using different polarizers in time as shown: The photodegradation can be controlled with the light chirality. (j) Corresponding experimental g-factors for the hybrids of panels (d,e,g,h). (k) Photochemical g-factors for the photodegradation data of panel (i). Copyrights for panels a and b*[61]*. Copyrights for panels c thru k*[60].

7. Some practice with 2D and 3D chiral objects.

The original definition of chirality should be applied, of course, to a 3D object. However, we use the term "2D chirality", which is convenient and serves the purpose. Figures 9a and 9b show chiral 2D patterns. In (a), we show a lateral nanostructure from one of the pioneering papers on chiroptics of metamaterials.[62] This structure is achiral in terms of 3D chirality and therefore the CD spectrum is inverted for the incident beams with k_z and $-k_z$. Figure 9b illustrates another type of a 2D

chiral patterns, which is a local phototemperature map.[63] In addition, electric fields and local field intensity often form chiral patterns in metastructures under illumination.[48,49]

The chirality of 2D and 3D objects is fundamentally different. The original 3D concept is more general and describes chiral molecules and colloidal NCs in the solution phase. In that case, we should assume that chiral objects are at random orientations. For lateral metamaterials and the normal light incidence, we talk about 2D chirality. Let's compare those cases. First, we look now at the properties of a scalar function, $\varphi(x,y,z)$. This function can be a local dielectric function of NC simply reflecting its shape, i.e., $\varepsilon(x,y,z)$, or it can be an electron density in a chiral molecule, i.e., $|\psi(x,y,z)|^2$. For example, $\varepsilon(x,y,z)$ and $|\psi(x,y,z)|^2$ can be of helical geometry, describing a plasmonic helix (e.g. Figures 2d-g, 4 or 7c) or an α-helix protein (e.g. Figures 1c or 3c). Next, we define chirality as an operator $\hat{C}$. The applications of this operator to a chiral function obey the following simple rules

$$\begin{aligned}
&\hat{C}\varphi(x,y,z) = +1\cdot\varphi(x,y,z)\\
&\hat{C}\varphi(-x,y,z) = -1\cdot\varphi(-x,y,z)\\
&\hat{C}\varphi(x,-y,z) = -1\cdot\varphi(x,-y,z)\\
&\hat{C}\varphi(x,y,-z) = -1\cdot\varphi(x,y,-z)\\
&\hat{C}\varphi(-x,-y,z) = (-1)^2\cdot\varphi(-x,-y,z)\\
&\ldots
\end{aligned} \qquad (6)$$

The above equalities are built using the following simple argument. Any inversion (mirror image) flips the chirality number. For example, the $\varphi(-x,y,z)$ function is a mirror image of $\varphi(x,y,z)$ and, therefore, it should be of inverted chirality, just like the RH and LH helices. According to eq 6, the chiral eigenvalues adopted here are $\lambda_C = \pm 1$. Really, the choice of λ_C is up to us. For

example, a RH helix may correspond to $\lambda_C = +1$, and a LH one may have $\lambda_C = -1$. Next, we consider a chiral object in the usual 3D coordinate space and apply the inversion-center operation,

$$\hat{P}_{3D}\varphi(x,y,z) = \varphi(-x,-y,-z),$$

and look its chirality. The operation means three mirror operations ($x \to -x$, $y \to -y$, $z \to -z$) and therefore:

$\hat{C} \cdot \hat{P}_{3D}\varphi(x,y,z) = (-1)^3 \varphi(-x,-y,-z) = -1 \cdot \varphi(-x,-y,-z)$. Simultaneously, it is obvious that $\hat{P}_{3D} \cdot \hat{C}\varphi(x,y,z) = +1 \cdot \varphi(-x,-y,-z)$, and we arrive to the anti-commutator property:

$$\left\{\hat{P}_{3D} \cdot \hat{C}\right\} = \hat{P}_{3D} \cdot \hat{C} + \hat{C} \cdot \hat{P}_{3D} = 0.$$

The above algebraic property simply means that a chiral object should not have the inversion-center symmetry, or the inversion-center operator (three mirrors) should create the opposite enantiomer. For the 2D case, however, we can only act within the x-y plane, and we immediately see fundamentally different properties: $\hat{C} \cdot \hat{P}_{2D}\varphi(x,y) = (-1)^2 \varphi(-x,-y) = +1 \cdot \varphi(-x,-y)$. Then, repeating the steps, we arrive to the commutator:

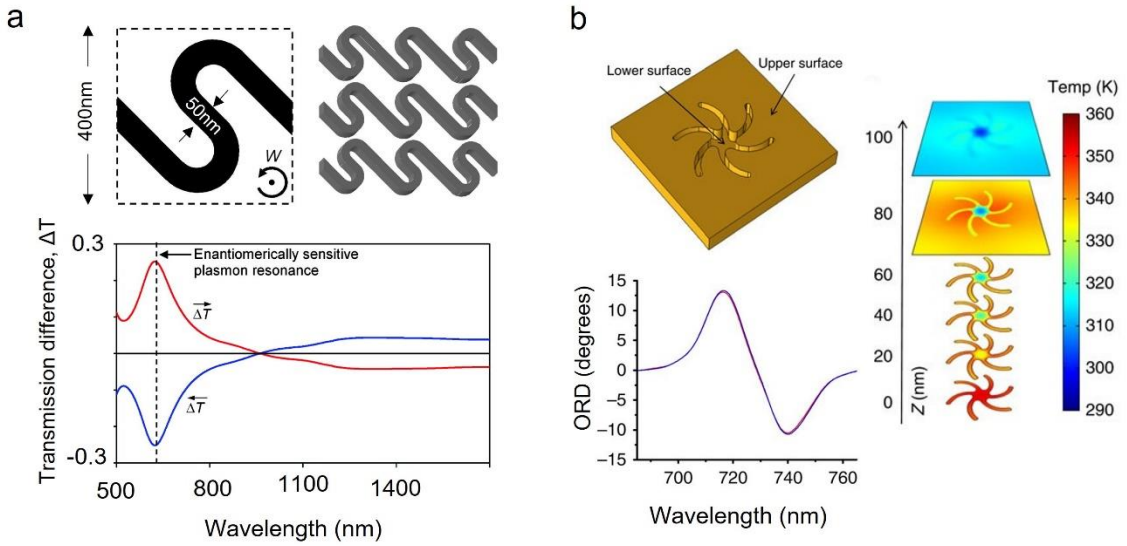
$$\left[\hat{P}_{2D} \cdot \hat{C}\right] = \hat{P}_{2D} \cdot \hat{C} - \hat{C} \cdot \hat{P}_{2D} = 0 .$$

This communication means that the inversion operation does change the chirality of a 2D object, but, simultaneously, the in-plane mirror operation flips the chirality, of course. Figure 9c-f illustrates those properties of the 2D world. The same conclusion is valid for the symmetry operations on the in-plane field patterns of CPL (bottom panels of Figures 9c-f, showing counterclockwise and clockwise symmetries). Those simple arguments provide the foundations

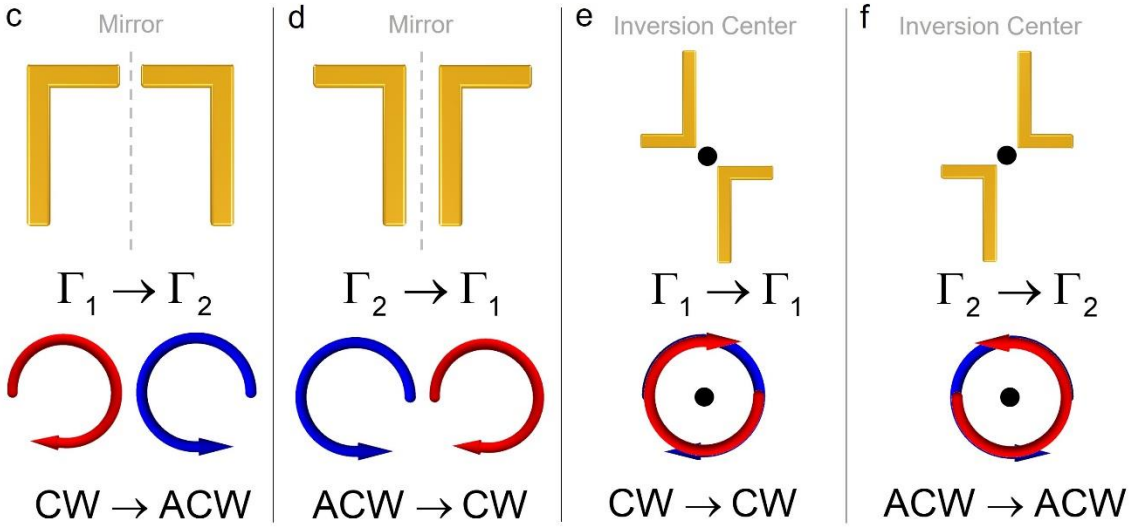
for the research field on planar chiral metamaterials with ultra-strong unidirectional CD signals. Here, however, one should make a remark. So far, we considered only the normal incidence case, whereas the geometry with titled incidence should be discussed separately in the context of so-called extrinsic chirality.[64]

The 2D World and directional CD in metastructures

Normal incidence – “2D chirality”



Mirror and inversion operations in 2D



Practice with periodic 2D chiral objects

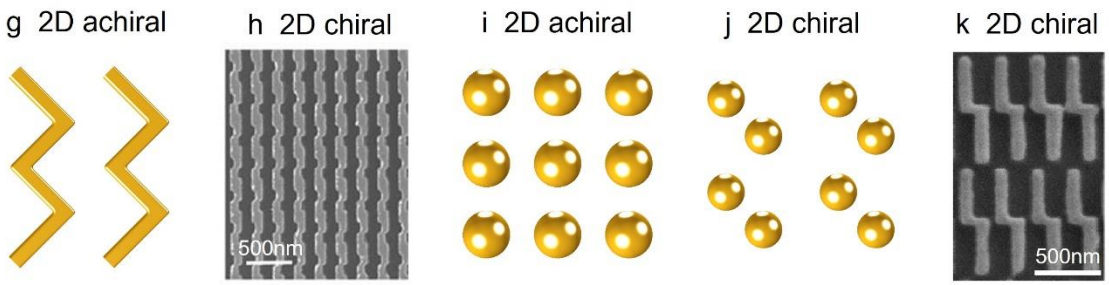


Figure 9: Directional CD in metastructures. *(a) Schematic of a continuous aluminum chiral "fish-scale" pattern structure, periodic in both directions (top panels), and relative enantiomeric difference in the total CPL transmission for forward (red) and backward (blue) direction of propagation (bottom panel), asymmetry which probes an enantiomerically sensitive plasmon. (b) Thermoplasmonic effect. A chiral plasmonic "shuriken" gold nanopatterned indentation (top left panel) embedded in a polycarbonate slide, and then covered in a continuous Au film, will generated different thermal gradients throughout z-cuts in the structure (right panel) upon laser irradiation. When an uncoated sample is irradiated, there are no changes in the optical rotatory dispersion (ORD) measurements (bottom left panel), whereas when the sample is coated, there is small ~1nm shift which indicates an structural change (not shown). (c-f) Different mirror and inversion operations in the simplest chiral 2D metastructure: an L-shape. (g-k) Different 2D arrangements of structures, both chiral and achiral as indicated. Copyright of panel a*[62]*. Copyright of panel b*[63]*. Copyright for panel h*[65]*. Copyright for panel k*[66]*.*

Finally, it is interesting to look at planar periodic metastructures and apply to them our 2D symmetry operations (Figures 9g-k). A simple zig-zag nanowire (NW) is achiral, even though its mirror image creates a formally different function, i.e., $\hat{R}_y\varphi(x,y)=\varphi(x,-y)\neq\varphi(x,y)$. Here, after the mirror operation, we have the liberty to shift our object and, in this way, superpose it. However, chiral zig-zag NWs can be created with more complex geometries, for example, like in Figure 9g. Finally, we can recall that there is a variety of bulk crystals with chiral lattices, such as Te, Se, HgS, etc. While single atoms in these materials are achiral, of course, these crystals possess strong chirality coming from the chiral arrangement of atoms. Similarly, planar metamaterials offer a possibility to design chiral lattices from achiral unit cells. Figure 9j shows one example of those,

which supports ultra-sharp lattice resonances and exhibit unique CD spectra.[67] Finally, we show an example of an achiral lattice with chiral unit cells[66] in Figure 9k; this structure from Ref. [66] demonstrated anonymously strong directional CD due to its clever chiral organization.

8. Conclusions and perspectives.

While coming from chemistry and biology,[1] the concept of geometrical chirality is now adopted widely in nanostructures, bio-conjugates, and metamaterials. A prominent optical phenomenon in biomolecules, CD, is a weak effect but very characteristic and amazingly sensitive to the molecular structure. In the solution setting, its theory requires simultaneous involvement of an electromagnetic wave's electric- and magnetic field components. In artificial nanostructures and bio-conjugates, the interactions of this kind become strongly enhanced because of the larger sizes and the ultra-strong plasmonic resonances. Moreover, biomolecules are mostly optically active in the UV interval for fundamental quantum reasons, whereas chiral plasmonic NCs show strong CD responses in the visible and near-IR regions. The bio-conjugates show the so-called plasmon-induced CD due to the exciton-plasmon interaction, and this effect can be used for sensing. A steady stream of publications in current literature concerns chiral NC assemblies fabricated using the DNA and protein linkers. It was exciting to see recent results on the optical chirality of a DNA-assembled helix with a continuously variable number of NCs.[29] The study of Ref. [29] has a few fundamental observations. The CD signal showed a clear threshold for $N_{\mathrm{NC}} = 4$, and the CD response never vanished even for $N_{\mathrm{NC}} < 4$. These observations in Ref. [29] are an example how chirality occurs at multiple scales and involves complex many-body interactions. Another intriguing possibility is plasmonic photochemistry with chiral colloidal NCs, which have optical

g-factors much greater than those in biomolecules. In this respect, one can notice two prominent production directions of research: (1) chiral growth using CPL and (2) chiral plasmonic photochemistry with achiral molecules combined with the chemical amplification effect. Regarding potential applications, one should mention chiral metamaterials for bio-sensing[17,68,69] and metasurfaces for efficient light manipulation.[70–72] Finally, we should note that the field of chiral inorganic and hybrid nanostructures is so active and involves so many research groups that many more research directions and scientific ideas should be expected to appear in the following years.

Notes

The authors declare no competing financial interest.

Acknowledgments

O.A.-O., G.M., and A.O.G acknowledge the generous support from the United States-Israel Binational Science Foundation (BSF). O.A.-O. and A.O.G are supported by the Nanoscale & Quantum Phenomena Institute at Ohio University. A.M and Z.M.W. acknowledge the National Key Research and Development Program of China (2019YFB2203400) and the "111 Project" (B20030). This work was also funded (M.A.C.-D.) by the Ministerio de Economía y Competitividad de España (CTM2017-84050-R), Xunta de Galicia (Centro Singular de Investigación de Galicia - Accreditation 2019-2022 ED431G 2019/06 and IN607A 2018/5), and European Union-ERDF (Interreg V-A - Spain-Portugal 0245_IBEROS_1_E, 0712_ACUINANO_1_E, and 0624_2IQBIONEURO_6_E, and Interreg Atlantic Area

NANOCULTURE 1.102.531). T. L. and K. M. acknowledge funding from the ERC consolidator grant “DNA functional lattices” (Project ID: 818635). In addition, the Munich-Ohio collaboration (i.e., T. L and A.O.G.) were generously supported from the Volkswagen Foundation. As for the support for the Zuse-Berlin group, S. B. acknowledges funding by the Deutsche Forschungsgemeinschaft under Germany´s Excellence Strategy – The Berlin Mathematics Research Center MATH+ (EXC-2046/1, project ID: 390685689) and by the German Federal Ministry of Education and Research (BMBF Forschungscampus MODAL, project number 05M20ZBM). Finally, A.O.G. appreciates the generous support from the Berlin MATH+ Center and Zuse-Institute Berlin via the 2021 MATH+ Distinguished Visiting Scholarship Award and the hospitality at Zuse-Berlin.

ORCID

Oscar Ávalos-Ovando: 0000-0003-3572-7675
Eva Yazmin Santiago: 0000-0001-8201-645X
Artur Movsesyan: 0000-0002-5425-7747
Peng Yu: 0000-0002-0242-7003
Lucas V. Besteiro: 0000-0001-7356-7719
Larousse Khosravi Khorashad: 0000-0003-0461-5638
Hiromi Okamoto: 0000-0003-0082-8652
Joseph M. Slocik: xxxx
Miguel A. Correa-Duarte: 0000-0003-1950-1414
Miguel Comesaña-Hermo: 0000-0001-8471-5510
Tim Liedl: 0000-0002-0040-0173
Zhiming Wang: 0000-0003-4171-1821
Gil Markovich: 0000-0002-4047-189X
Sven Burger: 0000-0002-3140-5380

Alexander O. Govorov: 0000-0003-1316-6758

References

(1) Bentley, R. From Optical Activity in Quartz to Chiral Drugs: Molecular Handedness in Biology and Medicine. *Perspectives in Biology and Medicine* **1995**, *38* (2), 188–229. https://doi.org/10.1353/pbm.1995.0069.

(2) Fasman, G. D. *Circular Dichroism and the Conformational Analysis of Biomolecules*, 1st ed.; Springer: Boston, MA, 1996.

(3) Rosenfeld, L. Quantenmechanische Theorie Der Natürlichen Optischen Aktivität von Flüssigkeiten Und Gasen. *Zeitschrift für Physik* **1929**, *52* (3), 161–174. https://doi.org/10.1007/BF01342393.

(4) Govorov, A. O. Plasmon-Induced Circular Dichroism of a Chiral Molecule in the Vicinity of Metal Nanocrystals. Application to Various Geometries. *J. Phys. Chem. C* **2011**, *115* (16), 7914–7923. https://doi.org/10.1021/jp1121432.

(5) Govorov, A. O.; Fan, Z.; Hernandez, P.; Slocik, J. M.; Naik, R. R. Theory of Circular Dichroism of Nanomaterials Comprising Chiral Molecules and Nanocrystals: Plasmon Enhancement, Dipole Interactions, and Dielectric Effects. *Nano Lett.* **2010**, *10* (4), 1374–1382. https://doi.org/10.1021/nl100010v.

(6) Zhang, H.; Govorov, A. O. Giant Circular Dichroism of a Molecule in a Region of Strong Plasmon Resonances between Two Neighboring Gold Nanocrystals. *Phys. Rev. B* **2013**, *87* (7), 075410. https://doi.org/10.1103/PhysRevB.87.075410.

(7) Besteiro, L. V.; Zhang, H.; Plain, J.; Markovich, G.; Wang, Z.; Govorov, A. O. Aluminum Nanoparticles with Hot Spots for Plasmon-Induced Circular Dichroism of Chiral Molecules in the UV Spectral Interval. *Advanced Optical Materials* **2017**, *5* (16), 1700069. https://doi.org/10.1002/adom.201700069.

(8) Kneer, L. M.; Roller, E.-M.; Besteiro, L. V.; Schreiber, R.; Govorov, A. O.; Liedl, T. Circular Dichroism of Chiral Molecules in DNA-Assembled Plasmonic Hotspots. *ACS Nano* **2018**, *12* (9), 9110–9115. https://doi.org/10.1021/acsnano.8b03146.

(9) Layani, M. E.; Ben Moshe, A.; Varenik, M.; Regev, O.; Zhang, H.; Govorov, A. O.; Markovich, G. Chiroptical Activity in Silver Cholate Nanostructures Induced by the Formation of Nanoparticle Assemblies. *J. Phys. Chem. C* **2013**, *117* (43), 22240–22244. https://doi.org/10.1021/jp400993j.

(10) Ben-Moshe, A.; Maoz, B. M.; Govorov, A. O.; Markovich, G. Chirality and Chiroptical Effects in Inorganic Nanocrystal Systems with Plasmon and Exciton Resonances. *Chem. Soc. Rev.* **2013**, *42* (16), 7028–7041. https://doi.org/10.1039/C3CS60139K.

(11) Slocik, J. M.; Govorov, A. O.; Naik, R. R. Plasmonic Circular Dichroism of Peptide-Functionalized Gold Nanoparticles. *Nano Lett.* **2011**, *11* (2), 701–705. https://doi.org/10.1021/nl1038242.

(12) Slocik, J. M.; Dennis, P. B.; Govorov, A. O.; Bedford, N. M.; Ren, Y.; Naik, R. R. Chiral Restructuring of Peptide Enantiomers on Gold Nanomaterials. *ACS Biomater. Sci. Eng.* **2020**, *6* (5), 2612–2620. https://doi.org/10.1021/acsbiomaterials.9b00933.

(13) Zhang Qingfeng; Hernandez Taylor; Smith Kyle W.; Hosseini Jebeli Seyyed Ali; Dai Alan X.; Warning Lauren; Baiyasi Rashad; McCarthy Lauren A.; Guo Hua; Chen Dong-Hua;

Dionne Jennifer A.; Landes Christy F.; Link Stephan. Unraveling the Origin of Chirality from Plasmonic Nanoparticle-Protein Complexes. *Science* **2019**, *365* (6460), 1475–1478. https://doi.org/10.1126/science.aax5415.
(14) Govorov, A. O.; Gun'ko, Y. K.; Slocik, J. M.; Gérard, V. A.; Fan, Z.; Naik, R. R. Chiral Nanoparticle Assemblies: Circular Dichroism, Plasmonic Interactions, and Exciton Effects. *J. Mater. Chem.* **2011**, *21* (42), 16806–16818. https://doi.org/10.1039/C1JM12345A.
(15) Cecconello, A.; Besteiro, L. V.; Govorov, A. O.; Willner, I. Chiroplasmonic DNA-Based Nanostructures. *Nature Reviews Materials* **2017**, *2* (9), 17039. https://doi.org/10.1038/natrevmats.2017.39.
(16) Kong, X.-T.; Besteiro, L. V.; Wang, Z.; Govorov, A. O. Plasmonic Chirality and Circular Dichroism in Bioassembled and Nonbiological Systems: Theoretical Background and Recent Progress. *Advanced Materials* **2020**, *32* (41), 1801790. https://doi.org/10.1002/adma.201801790.
(17) Link, S.; Hartland, G. V. Virtual Issue on Chiral Plasmonics. *J. Phys. Chem. C* **2021**, *125* (19), 10175–10178. https://doi.org/10.1021/acs.jpcc.1c03401.
(18) Fan, Z.; Govorov, A. O. Plasmonic Circular Dichroism of Chiral Metal Nanoparticle Assemblies. *Nano Lett.* **2010**, *10* (7), 2580–2587. https://doi.org/10.1021/nl101231b.
(19) Moffitt William. The Optical Rotatory Dispersion of Simple Polypeptides. II. *Proceedings of the National Academy of Sciences* **1956**, *42* (10), 736–746. https://doi.org/10.1073/pnas.42.10.736.
(20) Mastroianni, A. J.; Claridge, S. A.; Alivisatos, A. P. Pyramidal and Chiral Groupings of Gold Nanocrystals Assembled Using DNA Scaffolds. *J. Am. Chem. Soc.* **2009**, *131* (24), 8455–8459. https://doi.org/10.1021/ja808570g.
(21) Chen, W.; Bian, A.; Agarwal, A.; Liu, L.; Shen, H.; Wang, L.; Xu, C.; Kotov, N. A. Nanoparticle Superstructures Made by Polymerase Chain Reaction: Collective Interactions of Nanoparticles and a New Principle for Chiral Materials. *Nano Lett.* **2009**, *9* (5), 2153–2159. https://doi.org/10.1021/nl900726s.
(22) Fan, Z.; Zhang, H.; Govorov, A. O. Optical Properties of Chiral Plasmonic Tetramers: Circular Dichroism and Multipole Effects. *J. Phys. Chem. C* **2013**, *117* (28), 14770–14777. https://doi.org/10.1021/jp404987v.
(23) Kuzyk, A.; Schreiber, R.; Fan, Z.; Pardatscher, G.; Roller, E.-M.; Högele, A.; Simmel, F. C.; Govorov, A. O.; Liedl, T. DNA-Based Self-Assembly of Chiral Plasmonic Nanostructures with Tailored Optical Response. *Nature* **2012**, *483* (7389), 311–314. https://doi.org/10.1038/nature10889.
(24) Johnson, W. C.; Tinoco, I. Circular Dichroism of Polypeptide Solutions in the Vacuum Ultraviolet. *J. Am. Chem. Soc.* **1972**, *94* (12), 4389–4390. https://doi.org/10.1021/ja00767a084.
(25) Hu, L.; Liedl, T.; Martens, K.; Wang, Z.; Govorov, A. O. Long-Range Plasmon-Assisted Chiral Interactions in Nanocrystal Assemblies. *ACS Photonics* **2019**, *6* (3), 749–756. https://doi.org/10.1021/acsphotonics.8b01676.
(26) Shemer, G.; Krichevski, O.; Markovich, G.; Molotsky, T.; Lubitz, I.; Kotlyar, A. B. Chirality of Silver Nanoparticles Synthesized on DNA. *J. Am. Chem. Soc.* **2006**, *128* (34), 11006–11007. https://doi.org/10.1021/ja063702i.
(27) Shen, X.; Song, C.; Wang, J.; Shi, D.; Wang, Z.; Liu, N.; Ding, B. Rolling Up Gold Nanoparticle-Dressed DNA Origami into Three-Dimensional Plasmonic Chiral

Nanostructures. *J. Am. Chem. Soc.* **2012**, *134* (1), 146–149. https://doi.org/10.1021/ja209861x.
(28) Fan, Z.; Govorov, A. O. Helical Metal Nanoparticle Assemblies with Defects: Plasmonic Chirality and Circular Dichroism. *J. Phys. Chem. C* **2011**, *115* (27), 13254–13261. https://doi.org/10.1021/jp204265x.
(29) Martens, K.; Funck, T.; Santiago, E. Y.; Govorov, A. O.; Burger, S.; Liedl, T. On the Origin of Chirality in Plasmonic Meta-Molecules. arXiv: 2110.06689 2022.
(30) Govorov, A. O.; Fan, Z. Theory of Chiral Plasmonic Nanostructures Comprising Metal Nanocrystals and Chiral Molecular Media. *ChemPhysChem* **2012**, *13* (10), 2551–2560. https://doi.org/10.1002/cphc.201100958.
(31) Artur Movsesyan; Santiago, E. Y.; Burger, S.; Correa-Duarte, M. A.; Besteiro, L. V.; Wang, Z.; Govorov, A. O. Plasmonic Nanocrystals with Complex Shapes for Photocatalysis and Growth: Contrasting Anisotropic Hot-Electron Generation with the Photothermal Effect. arXiv: 2203.00930 2022.
(32) Pasteur, L. Researches on the Molecular Asymmetry of Natural Organic Products, L. Pasteur (Alembic Club Reprints 1905). In *Selected Papers on Natural Optical Activity*; 1990; Vol. MS15, p 624.
(33) Eliel, E. L.; Wilen, S. H. *Stereochemistry of Organic Compounds*, 1st ed.; Wiley, 1994.
(34) Article "Helix", Https://En.Wikipedia.Org/Wiki/Helix.
(35) Cathcart, N.; Kitaev, V. Monodisperse Hexagonal Silver Nanoprisms: Synthesis via Thiolate-Protected Cluster Precursors and Chiral, Ligand-Imprinted Self-Assembly. *ACS Nano* **2011**, *5* (9), 7411–7425. https://doi.org/10.1021/nn2023478.
(36) Ben-Moshe, A.; Govorov, A. O.; Markovich, G. Enantioselective Synthesis of Intrinsically Chiral Mercury Sulfide Nanocrystals. *Angewandte Chemie International Edition* **2013**, *52* (4), 1275–1279. https://doi.org/10.1002/anie.201207489.
(37) Ben-Moshe, A.; Wolf, S. G.; Sadan, M. B.; Houben, L.; Fan, Z.; Govorov, A. O.; Markovich, G. Enantioselective Control of Lattice and Shape Chirality in Inorganic Nanostructures Using Chiral Biomolecules. *Nature Communications* **2014**, *5* (1), 4302. https://doi.org/10.1038/ncomms5302.
(38) Fan, Z.; Govorov, A. O. Chiral Nanocrystals: Plasmonic Spectra and Circular Dichroism. *Nano Lett.* **2012**, *12* (6), 3283–3289. https://doi.org/10.1021/nl3013715.
(39) Lee, H.-E.; Ahn, H.-Y.; Mun, J.; Lee, Y. Y.; Kim, M.; Cho, N. H.; Chang, K.; Kim, W. S.; Rho, J.; Nam, K. T. Amino-Acid- and Peptide-Directed Synthesis of Chiral Plasmonic Gold Nanoparticles. *Nature* **2018**, *556* (7701), 360–365. https://doi.org/10.1038/s41586-018-0034-1.
(40) Negrín-Montecelo, Y.; Comesaña-Hermo, M.; Khorashad, L. K.; Sousa-Castillo, A.; Wang, Z.; Pérez-Lorenzo, M.; Liedl, T.; Govorov, A. O.; Correa-Duarte, M. A. Photophysical Effects behind the Efficiency of Hot Electron Injection in Plasmon-Assisted Catalysis: The Joint Role of Morphology and Composition. *ACS Energy Lett.* **2020**, *5* (2), 395–402. https://doi.org/10.1021/acsenergylett.9b02478.
(41) Tsoulos, T. V.; Atta, S.; Lagos, M. J.; Beetz, M.; Batson, P. E.; Tsilomelekis, G.; Fabris, L. Colloidal Plasmonic Nanostar Antennas with Wide Range Resonance Tunability. *Nanoscale* **2019**, *11* (40), 18662–18671. https://doi.org/10.1039/C9NR06533D.
(42) Okamoto, H. Local Optical Activity of Nano- to Microscale Materials and Plasmons. *J. Mater. Chem. C* **2019**, *7* (47), 14771–14787. https://doi.org/10.1039/C9TC05141D.

(43) Narushima, T.; Okamoto, H. Strong Nanoscale Optical Activity Localized in Two-Dimensional Chiral Metal Nanostructures. *J. Phys. Chem. C* **2013**, *117* (45), 23964–23969. https://doi.org/10.1021/jp409072h.
(44) Kong, X.-T.; Khosravi Khorashad, L.; Wang, Z.; Govorov, A. O. Photothermal Circular Dichroism Induced by Plasmon Resonances in Chiral Metamaterial Absorbers and Bolometers. *Nano Lett.* **2018**, *18* (3), 2001–2008. https://doi.org/10.1021/acs.nanolett.7b05446.
(45) Spaeth, P.; Adhikari, S.; Le, L.; Jollans, T.; Pud, S.; Albrecht, W.; Bauer, T.; Caldarola, M.; Kuipers, L.; Orrit, M. Circular Dichroism Measurement of Single Metal Nanoparticles Using Photothermal Imaging. *Nano Lett.* **2019**, *19* (12), 8934–8940. https://doi.org/10.1021/acs.nanolett.9b03853.
(46) Rafiei Miandashti, A.; Khosravi Khorashad, L.; Kordesch, M. E.; Govorov, A. O.; Richardson, H. H. Experimental and Theoretical Observation of Photothermal Chirality in Gold Nanoparticle Helicoids. *ACS Nano* **2020**, *14* (4), 4188–4195. https://doi.org/10.1021/acsnano.9b09062.
(47) Hashiyada, S.; Narushima, T.; Okamoto, H. Imaging Chirality of Optical Fields near Achiral Metal Nanostructures Excited with Linearly Polarized Light. *ACS Photonics* **2018**, *5* (4), 1486–1492. https://doi.org/10.1021/acsphotonics.7b01511.
(48) Saito, K.; Tatsuma, T. Chiral Plasmonic Nanostructures Fabricated by Circularly Polarized Light. *Nano Lett.* **2018**, *18* (5), 3209–3212. https://doi.org/10.1021/acs.nanolett.8b00929.
(49) Horrer, A.; Zhang, Y.; Gérard, D.; Béal, J.; Kociak, M.; Plain, J.; Bachelot, R. Local Optical Chirality Induced by Near-Field Mode Interference in Achiral Plasmonic Metamolecules. *Nano Lett.* **2020**, *20* (1), 509–516. https://doi.org/10.1021/acs.nanolett.9b04247.
(50) Li Yuanwei; Lin Haixin; Zhou Wenjie; Sun Lin; Samanta Devleena; Mirkin Chad A. Corner-, Edge-, and Facet-Controlled Growth of Nanocrystals. *Science Advances 7* (3), eabf1410. https://doi.org/10.1126/sciadv.abf1410.
(51) Guo, W.; Johnston-Peck, A. C.; Zhang, Y.; Hu, Y.; Huang, J.; Wei, W. D. Cooperation of Hot Holes and Surface Adsorbates in Plasmon-Driven Anisotropic Growth of Gold Nanostars. *J. Am. Chem. Soc.* **2020**, *142* (25), 10921–10925. https://doi.org/10.1021/jacs.0c03342.
(52) Besteiro, L. V.; Movsesyan, A.; Ávalos-Ovando, O.; Lee, S.; Cortés, E.; Correa-Duarte, M. A.; Wang, Z. M.; Govorov, A. O. Local Growth Mediated by Plasmonic Hot Carriers: Chirality from Achiral Nanocrystals Using Circularly Polarized Light. *Nano Lett.* **2021**, *21* (24), 10315–10324. https://doi.org/10.1021/acs.nanolett.1c03503.
(53) Khorashad, L. K.; Besteiro, L. V.; Correa-Duarte, M. A.; Burger, S.; Wang, Z. M.; Govorov, A. O. Hot Electrons Generated in Chiral Plasmonic Nanocrystals as a Mechanism for Surface Photochemistry and Chiral Growth. *J. Am. Chem. Soc.* **2020**, *142* (9), 4193–4205. https://doi.org/10.1021/jacs.9b11124.
(54) Rau, L. H. Direct Asymmetric Photochemistry with Circularly Polarized Light. In *Chiral Photochemistry*; CRC Press: Boca Raton, 2004; p 704.
(55) Le Bel, J. A. Sur Les Relations Qui Existent Entre Les Formules Atomiques Des Corps Organiques et Le Pouvoir Rotatoire de Leurs Dissolutions. *Bulletin de la Société Chimique de Paris* **1874**, *22*, 337–347.
(56) van 'T Hoff, J. H. *Die Lagerung Der Atome Im Raum*, 2nd ed.; F. Vieweg, 1894.

(57) Kuhn, W.; Braun, E. Photochemische Erzeugung Optisch Aktiver Stoffe. *Naturwissenschaften* **1929**, *17* (14), 227–228.
(58) Kuhn, W.; Knopf, E. The Preparation of Optically Active Compounds by the Aid of Light. *Z. Physik. Chem* **1930**, *7*, 292–310.
(59) Kim, J.-Y.; Yeom, J.; Zhao, G.; Calcaterra, H.; Munn, J.; Zhang, P.; Kotov, N. Assembly of Gold Nanoparticles into Chiral Superstructures Driven by Circularly Polarized Light. *J. Am. Chem. Soc.* **2019**, *141* (30), 11739–11744. https://doi.org/10.1021/jacs.9b00700.
(60) Negrín-Montecelo, Y.; Movsesyan, A.; Gao, J.; Burger, S.; Wang, Z. M.; Nlate, S.; Pouget, E.; Oda, R.; Comesaña-Hermo, M.; Govorov, A. O.; Correa-Duarte, M. A. Chiral Generation of Hot Carriers for Polarization-Sensitive Plasmonic Photocatalysis. *J. Am. Chem. Soc.* **2022**, *144* (4), 1663–1671. https://doi.org/10.1021/jacs.1c10526.
(61) Liu, T.; Besteiro, L. V.; Liedl, T.; Correa-Duarte, M. A.; Wang, Z.; Govorov, A. O. Chiral Plasmonic Nanocrystals for Generation of Hot Electrons: Toward Polarization-Sensitive Photochemistry. *Nano Lett.* **2019**, *19* (2), 1395–1407. https://doi.org/10.1021/acs.nanolett.8b05179.
(62) Fedotov, V. A.; Schwanecke, A. S.; Zheludev, N. I.; Khardikov, V. V.; Prosvirnin, S. L. Asymmetric Transmission of Light and Enantiomerically Sensitive Plasmon Resonance in Planar Chiral Nanostructures. *Nano Lett.* **2007**, *7* (7), 1996–1999. https://doi.org/10.1021/nl0707961.
(63) Jack, C.; Karimullah, A. S.; Tullius, R.; Khorashad, L. K.; Rodier, M.; Fitzpatrick, B.; Barron, L. D.; Gadegaard, N.; Lapthorn, A. J.; Rotello, V. M.; Cooke, G.; Govorov, A. O.; Kadodwala, M. Spatial Control of Chemical Processes on Nanostructures through Nano-Localized Water Heating. *Nature Communications* **2016**, *7* (1), 10946. https://doi.org/10.1038/ncomms10946.
(64) Collins, J. T.; Kuppe, C.; Hooper, D. C.; Sibilia, C.; Centini, M.; Valev, V. K. Chirality and Chiroptical Effects in Metal Nanostructures: Fundamentals and Current Trends. *Advanced Optical Materials* **2017**, *5* (16), 1700182. https://doi.org/10.1002/adom.201700182.
(65) Li, W.; Coppens, Z. J.; Besteiro, L. V.; Wang, W.; Govorov, A. O.; Valentine, J. Circularly Polarized Light Detection with Hot Electrons in Chiral Plasmonic Metamaterials. *Nature Communications* **2015**, *6* (1), 8379. https://doi.org/10.1038/ncomms9379.
(66) Ouyang, L.; Wang, W.; Rosenmann, D.; Czaplewski, D. A.; Gao, J.; Yang, X. Near-Infrared Chiral Plasmonic Metasurface Absorbers. *Opt. Express* **2018**, *26* (24), 31484–31489. https://doi.org/10.1364/OE.26.031484.
(67) Movsesyan, A.; Besteiro, L. V.; Kong, X.-T.; Wang, Z.; Govorov, A. O. Engineering Strongly Chiral Plasmonic Lattices with Achiral Unit Cells for Sensing and Photodetection. *Advanced Optical Materials* **2021**, *n/a* (n/a), 2101943. https://doi.org/10.1002/adom.202101943.
(68) Hendry, E.; Carpy, T.; Johnston, J.; Popland, M.; Mikhaylovskiy, R. V.; Lapthorn, A. J.; Kelly, S. M.; Barron, L. D.; Gadegaard, N.; Kadodwala, M. Ultrasensitive Detection and Characterization of Biomolecules Using Superchiral Fields. *Nature Nanotechnology* **2010**, *5* (11), 783–787. https://doi.org/10.1038/nnano.2010.209.
(69) Abdulrahman, N. A.; Fan, Z.; Tonooka, T.; Kelly, S. M.; Gadegaard, N.; Hendry, E.; Govorov, A. O.; Kadodwala, M. Induced Chirality through Electromagnetic Coupling between Chiral Molecular Layers and Plasmonic Nanostructures. *Nano Lett.* **2012**, *12* (2), 977–983. https://doi.org/10.1021/nl204055r.

(70) Gorkunov, M. V.; Antonov, A. A.; Kivshar, Y. S. Metasurfaces with Maximum Chirality Empowered by Bound States in the Continuum. *Phys. Rev. Lett.* **2020**, *125* (9), 093903. https://doi.org/10.1103/PhysRevLett.125.093903.
(71) Plum, E.; Zheludev, N. I. Chiral Mirrors. *Appl. Phys. Lett.* **2015**, *106* (22), 221901. https://doi.org/10.1063/1.4921969.
(72) Chen, Y.; Du, W.; Zhang, Q.; Ávalos-Ovando, O.; Wu, J.; Xu, Q.-H.; Liu, N.; Okamoto, H.; Govorov, A. O.; Xiong, Q.; Qiu, C.-W. Multidimensional Nanoscopic Chiroptics. *Nature Reviews Physics* **2022**, *4* (2), 113–124. https://doi.org/10.1038/s42254-021-00391-6.